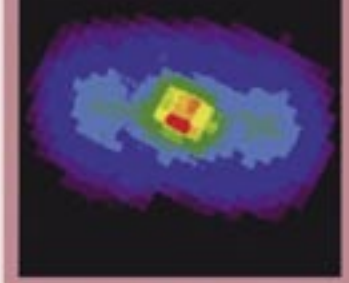

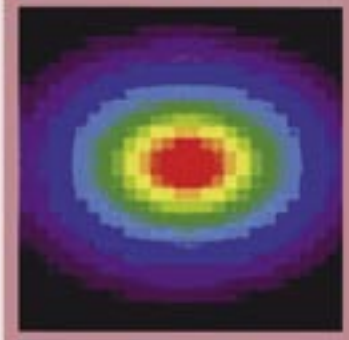

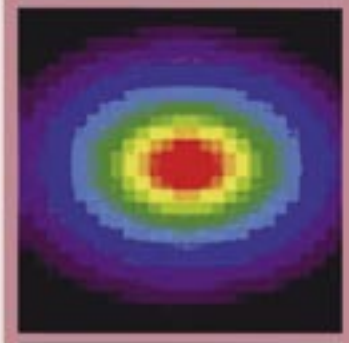

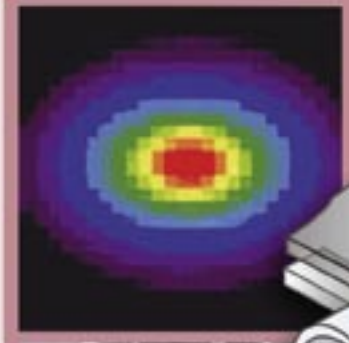

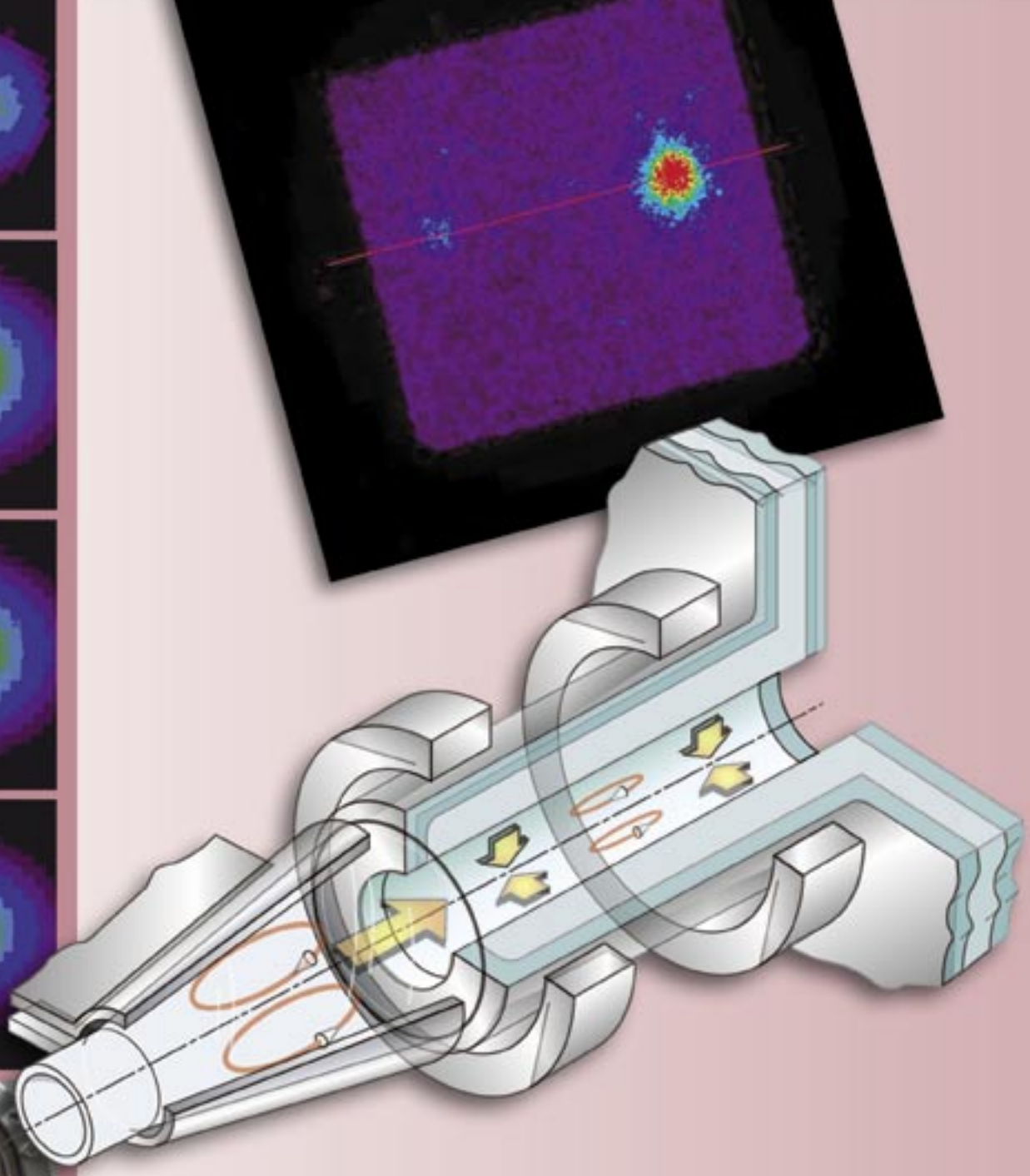

$$\delta_{ph} = (\lambda \Sigma \tan\theta \Sigma 1n2 + D_{clr})\left(1 + \frac{1}{M}\right)$$

$$p\frac{d}{dt}\left(\frac{p_i}{p}(u_i - u)\right) + \Sigma_j \frac{p_i p_j}{p} v_{ij}(u_i - u_j) = -p_i(u_i - u)\Sigma \nabla u -$$

Plasma Physics

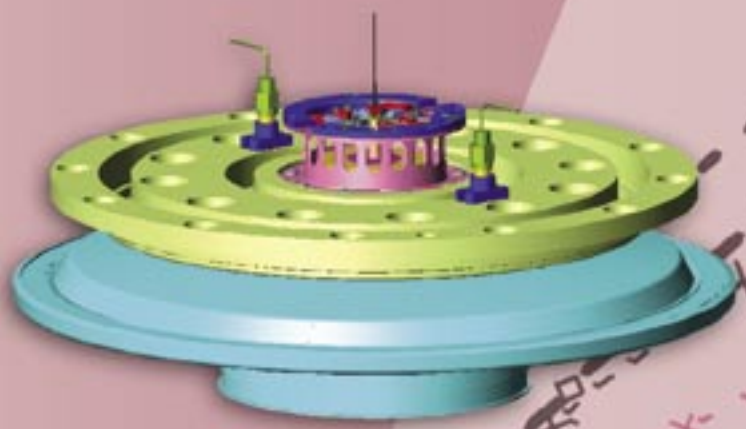

$$\nabla \Sigma P_i + \frac{p_i}{p} \nabla \Sigma P$$

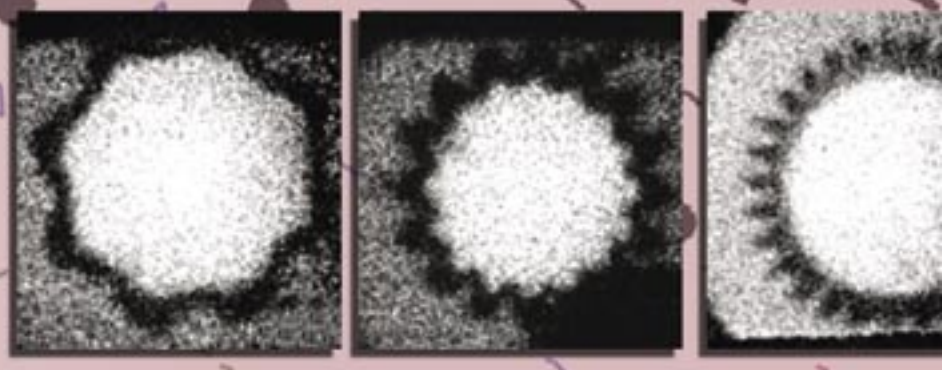

Plasma Physics Contents

Research Highlights

Project Descriptions

Understanding the Richtmyer-Meshkov Instability in the High-Energy-Density Regime

S.H. Batha, M.M. Balkey, C.W. Barnes, J.R. Fincke, N.E. Lanier (P-24), N.D. Delamater, R.M. Hueckstaedt, G.R. Magelssen, J.M. Scott (X-2), R.D. Day (MST-7), A.M. Dunne, C.J. Horsfield, K.W. Parker, S.D. Rothman (Atomic Weapons Establishment)

Fusion, the process that produces thermonuclear reactions in the sun, may someday be a solution to the world's energy problem as a virtually inexhaustible, relatively clean, and cost-effective energy source. For several decades, researchers worldwide have been investigating several approaches to initiate and control thermonuclear reactions. These methods involve the creation of a hot, dense plasma (an electrically conducting fluid composed of freely moving ions and electrons) heated to millions of degrees and held together long enough to produce useful energy through fusion reactions. One method (ICF)[1] implodes a pearl-size spherical capsule (a common geometry used in ICF experiments) that contains fusion fuel: deuterium (D) and tritium (T). Laser energy (or x-rays generated by the lasers) is deposited on the outside of the capsule, which ablates and drives shocks in towards the DT fuel. The fuel is ignited and burns for less than a billionth of a second. Ideally, the inertia of the highly dense plasma should hold it together long enough to produce fusion conditions. But achieving sustained thermonuclear fusion under laboratory conditions is difficult and has therefore become a "Grand Challenge" problem for the U.S. science community.

As shocks pass through material interfaces, they create Richtmyer-Meshkov Instabilities (RMI)[2,3] that "mix" the different materials. In *high-energy-density* ICF experiments using the Omega laser[4] at the LLE (University of Rochester), researchers are performing a series of implosion experiments to gain a better understanding of RMI. If not mitigated, the RMI creates "mixing" that introduces impurities into the fusion fuel. Impurities can dilute and cool the fusion fuel and quench the thermonuclear reaction. Although the typical ignition capsule used in ICF experiments is spherical, measuring the extent of mix at target interfaces in a sphere is difficult, if not impossible. For our RMI experiments, we used a cylindrical target that allows us to measure and observe mix axially along the interfaces while they are converging.

Understanding "Mix" in Fusion Reactions

The target assemblies used in our experiments were composed of materials with different densities (Figure 1). In each assembly, a small epoxy cylinder (outer target layer) was filled with polystyrene foam (inner target layer); an aluminum marker band with corrugations (perturbations) in its outer surface was inserted between the epoxy cylinder and the foam (Figure 1). The areas subject to RMI in these experiments involved two regions on the target assembly: (1) the interface between the epoxy cylinder and the marker band and (2) the interface between the marker band and the foam.

Fifty of the 60 Omega lasers illuminate the target assemblies with 18 kJ of energy. This energy heats them to extreme temperatures causing approximately one-half of the epoxy cylinder to vaporize and expand outward (away from the cylinder), while the other half is pushed inward (implodes) by a strong shock wave—a pressure force that travels faster than the speed of sound in the

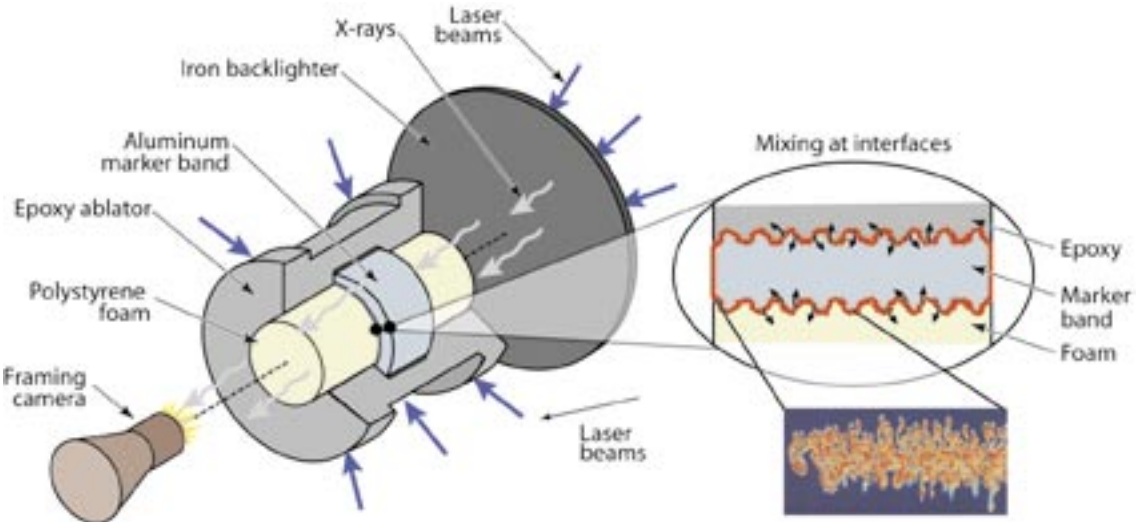

Figure 1. Rendering of a typical target used in the RMI experiment. These targets are about 2.25 mm long and 1 mm in diameter. A rough surface is machined into the outside of the aluminum marker band. The inset shows mixing at the interfaces. The target below (oriented in the same position as the rendering of the target) and an image of "mix" obtained from an advanced simulation are shown.

material. The passage of the shock wave through the target assembly heats the target materials and causes them to become plasmas. As a result, the interfaces along both sides of the marker band are accelerated, and the materials mix over time. The danger of RMI is that if the mixing becomes severe enough in an ignition capsule, fusion reactions end, and thermonuclear ignition—the ultimate goal of all ICF experiments—fails. To measure the amount of mixing, 5 additional laser beams from Omega strike an iron foil at one end of the cylinder after a small time delay. X-rays are emitted, travel lengthwise through the cylinder, and are collected by a framing camera that records 16 images through a pinhole. Each image spans approximately 60 ps, and the 16 images are distributed over 1 ns.[5]

Richtmyer-Meshkov Instability

The Richtmyer-Meshkov instability is a hydrodynamic instability driven by the passage of a strong shock past an interface between two fluids. Any perturbation present at the interface will grow proportionately with time. Most previous research into RMI has been done with intentionally seeded, simple perturbations in a flat geometry. Our recent high-energy-density RMI experiments[6,7] had several distinct features over these other RMI experiments. We imploded a cylindrical target to capture the same effects of a *convergent* geometry as those in an ICF capsule implosion. The target material in our RMI experiment was *compressible*—that is, the density increased when the shock passed through it. In addition, the materials that comprised the composite target in our experiments were *miscible* and could therefore mix freely into one another.

Moreover, we were interested in studying the effects of shock waves in the *strong-shock* regime where Mach (supersonic) numbers are greater than 10. With such strong shocks, the RMI grows in proportion to the Mach number. Finally, the Reynolds number was about 1 million, which placed the fluid flow well into the turbulent fluid regime. (In fluid mechanics, the Reynolds number is the ratio of inertial to viscous forces. A high Reynolds number means that the flow can become turbulent because the viscosity of the fluid does not damp the effects of any local disturbance.) Currently, no accepted theoretical or computational model exists for explaining such complex environments. Experimental data in such regimes are needed if controlled thermonuclear fusion energy is eventually to become a reality.

The critical measurement and signature of the RMI in this experiment is the expansion of the interfaces of the radiographically opaque marker band into both the foam and epoxy. A typical datum is displayed in Figure 2a in which the transmissive inner foam, the opaque marker band, and the translucent epoxy outer layer are visible. Data in these experiments were azimuthally averaged to make quantitative comparisons with advanced computer simulations. The width of the marker layer is defined as the difference between the inner and outer 50% transmission points (Figure 2b), and systematic parallax effects are removed. By analyzing each of the 16 images obtained in one experiment and then repeating the experiment with different measurement timing, we can record an entire implosion history (Figure 3).

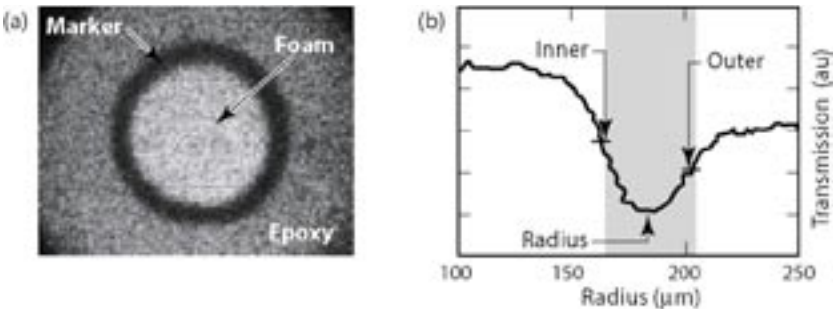

Figure 2. A radiographic image of a smooth aluminum marker (a). The average radial profile (b) is obtained from an azimuthal average of the transmission.

The computer modeling used in the RMI experiments excellently reproduced the marker widths and the position of the marker bands with initially very smooth marker surfaces. Both the experiment and the code show a steady increase in the marker width as the cylinder implodes, reaching a maximum width when the cylinder has reached minimum volume. As the cylinder "bounces" or expands, the marker width decreases.

The key scientific question that we are trying to answer is how do surface imperfections—that is, the initial conditions—affect the evolution of the RMI? We addressed this question by machining surface features (like the thread of a screw) along the length of the outer surface of the aluminum marker band. Surface perturbations like these produce a much wider marker band than do initially smooth bands (Figure 2). Randomly rough surfaces are not seen to mix any more than initially smooth surfaces.

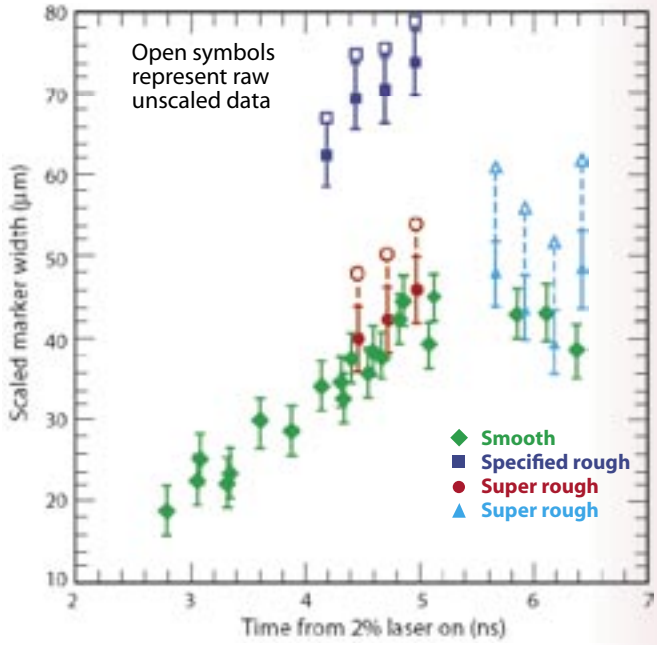

Figure 3. The measured marker-width evolution shows that the marker increases in width until about 5 ns when the cylinder reaches maximum compression. The data points at even larger marker widths are for targets that had the marker surface prepared in a particular manner (i.e., screw thread) to enhance mixing.

A conceptually much simpler outer surface is an azimuthally varying sinusoidal surface, like a tube with corrugations running the length of the tube.[8] This direct analog to numerous planar experiments is readily simulated with several different advanced computational codes and is potentially tractable theoretically. Such targets have been manufactured and experimentally tested. Figure 4 shows the experimental data from three experiments where the number of oscillations was 8, 16, or 28. The initial peak-to-valley size of the perturbation (6 μm) was the same for each experiment. Based on measurements and modeling of planar experiments, we expected that the size of the perturbations in our experiments would be directly dependent on the number of initial perturbations. In other words, we expected the growth in the 28-perturbation target to be 3.5 times larger than the 8-perturbation target at the same time. However, as shown in the data of Figure 4, this did not happen. In fact, the perturbations in all three cases (the 8, 16, or 28 perturbation targets) have approximately the same amplitude. Simulations using complex codes actually predicted the same trend. We are still determining the physical reason for these results in ongoing work.

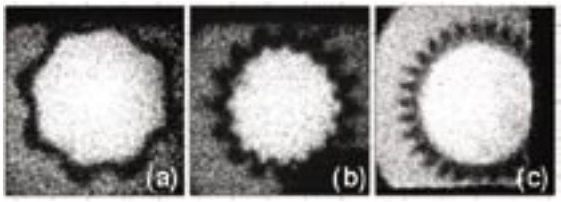

Figure 4. Axial radiographs of single-mode sinusoidally perturbed targets with mode numbers of 8 (a), 16 (b), and 28 (c).

Conclusion

The fundamental physical explanation for these results—that some types of surfaces grow whereas others do not when a strong shock is applied—is not known. Our experiments found that the type of perturbation at the interface affected the subsequent level of instability growth. Computer simulations were able to reproduce some of the results (Figure 4) but not others (Figure 3). We are pursuing experimental and computational lines of inquiry to understand the physics and modeling of these simplified experiments. Computational modeling is using features of the advanced codes, such as modern mix models and three-dimensional simulations, to address these issues. Experimentally, we implemented improvements to the framing-camera diagnostic to improve its spatial resolution. These improvements seem to have increased the quantitative accuracy of these experiments. We are also pursuing focused experiments on the effect of perturbation wavelength. Besides full-surface perturbations, the effects of material defects, like those seen at the joint of a beryllium capsule during implosion, are being investigated. Finally, we are measuring the effect of a second shock on the marker layer. Future experiments in convergent, compressible fluid instabilities in the presence of strong shocks are being planned for the NIF.[9] These cylinders will be imploded by soft x-ray radiation, which will allow faster implosion velocities, the use of larger cylinders, and better relative resolution of the mixing zone.

References

1. J.D. Lindl, *Inertial confinement fusion: The quest for ignition and energy gain using indirect drive* (Springer, New York, 1998).
2. R.D. Richtmyer, "Taylor instability in shock acceleration of compressible fluids," *Communications on Pure and Applied Mathematics* **13**, 297 (1960).
3. E. Meshkov, "Instability of the interface of two gases accelerated by a shock wave," *Soviet Fluid Dynamics* **4**, 101 (1969).
4. T.R. Boehly, D.L. Brown, R.S. Craxton, R.L. Keck, J.P. Knauer, J.H. Kelly, T.J. Kessler, S.A. Kumpan, S.J. Loucks, S.A. Letzring, F.J. Marshall, R.L. McCrory, S.F.B. Morse, W. Seka, J.M. Soures, and C.P. Verdon, "Initial performance results of the Omega laser system," *Optics Communications* **133**, 495 (1997).
5. J.D. Kilkenny, "High-speed proximity focused x-ray cameras," *Laser and Particle Beams* **9**, 49 (1991).
6. C.W. Barnes, S.H. Batha, A.M. Dunne, G. R. Magelssen, S.D. Rothman, R.D. Day, N.E. Elliott, D.A. Haynes, R.L. Holmes, J.M. Scott, D.L. Tubbs, D.L. Youngs, T.R. Boehly, and P. Jaanimagi, "Observation of mix in a compressible plasma in a convergent cylindrical geometry," *Physics of Plasmas* **9**, 4431 (2002).
7. N.E. Lanier, C.W. Barnes, S.H. Batha, R.D. Day, G.R. Magelssen, J.M. Scott, A.M. Dunne, K.W. Parker, and S.D. Rothman, "Multi-mode seeded Richtmyer-Meshkov mixing in a convergent, compressible, miscible plasma system," *Physics of Plasmas* **10**, 1816 (2003).
8. M.M. Balkey, R.D. Day, S.H. Batha, N.E. Elliott, T. Pierce, D.L. Sandoval, K.P. Garrard, and A. Sohn, "Production and metrology of cylindrical inertial confinement fusion targets with sinusoidal perturbations," Los Alamos National Laboratory report LA-UR-03-3682 (2003); to be published in *Fusion Science and Technology* (2003).
9. E.M. Campbell and W.J. Hogan, "The national ignition facility—applications for inertial fusion energy and high-energy-density science," *Plasma Physics and Controlled Fusion* **41** (12B, B39) (1999).

Acknowledgment

The RMI experiments are a collaborative effort between LANL and the AWE and are sponsored by the DOE NNSA.

For more information, contact Steven Batha at 505-665-5898, sbatha@lanl.gov.

Neutron Pinhole Imaging for Inertial-Confinement-Fusion Experiments

G.P. Grim, G.L. Morgan, M.D. Wilke (P-23), P.L. Gobby (MST-7), C.R. Christensen (P-24), D.C. Wilson (X-2)

The technique of imaging via pinhole is simple and yet remarkably powerful. Because of its simplicity, its basic optical principles have been considered for nearly three thousand years. As early as the fifth century B.C., Chinese philosophers used the pinhole to demonstrate the linearity of light propagation. Over the course of the next two millennia, notables, such as Aristotle, Leonardo da Vinci, and Johannes Kepler, among others, conducted studies with pinholes to advance knowledge in the field of astronomy. These studies included the imaging of solar eclipses and the determination of the correct day of the vernal equinox.

The first use of the pinhole technique to image neutrons from the fusion of deuterium and tritium occurred in April 1957 on the Boltzman shot during the early stages of nuclear weapons development in the U.S. Because of the penetrating nature of neutrons, the pinhole apparatus was modified, but the technique was fundamentally the same as for imaging light. In a typical neutron-pinhole experiment[1-4] (Figure 1), neutrons from a source that is to be imaged impinge upon a pinhole assembly and are either transported without scattering to the detector, or they interact within the assembly and are not recorded. In the experiments presented here, the neutrons are detected when they interact in a 3-cm-diam by 5-cm-long bundle of 0.5-mm-diam scintillating fibers. The scintillation light from the neutron interactions within the bundled fibers is totally internally reflected along the fibers and coupled into a series of coherent fiber-optical-transport elements. After the light passes through these elements, it is captured by a CCD camera and recorded in digital form on a computer for later analysis.

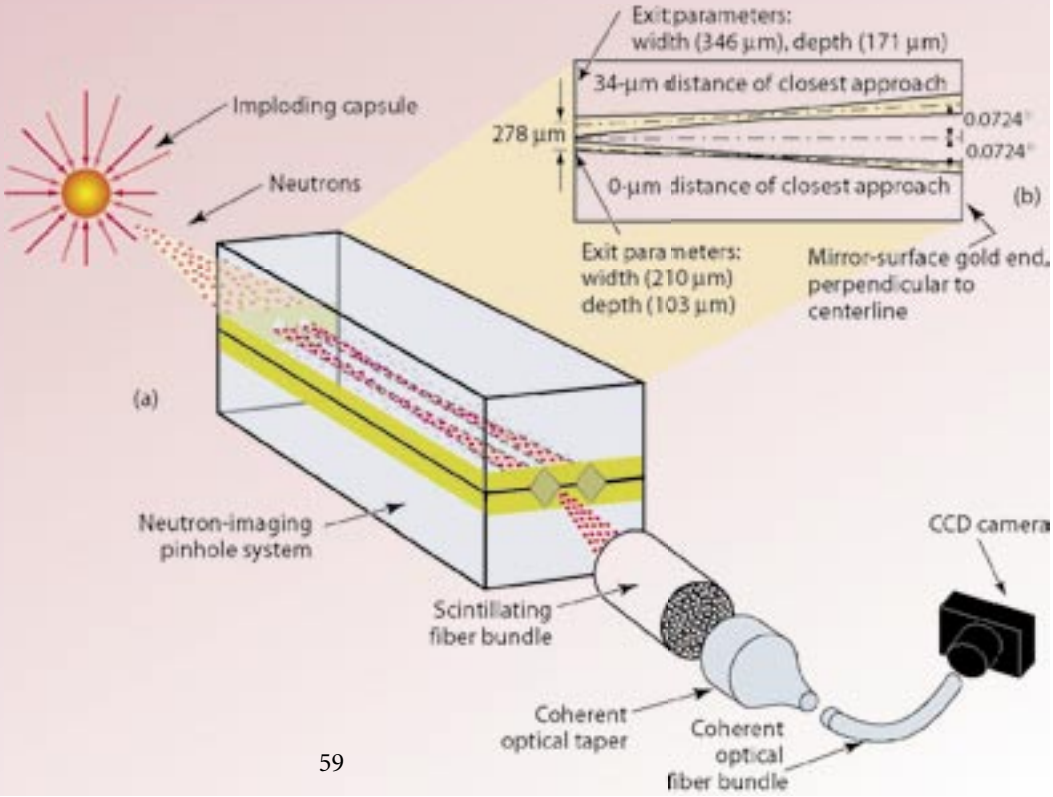

Figure 1. Typical pinhole neutron experiment. Figure 1(a) is a rendering of a typical implosion shot, and Figure 1(b) is the schematic of the pinhole apparatus used in the experiments on the Omega laser.

Figure 2. Inside the target chamber of the Omega laser. The bright spot at the center of the chamber is the light produced from imploding a DT capsule on shot 31184. The elements protruding from the wall include various x-ray and neutron diagnostics and the neutron pinhole used for the experiments described herein.

During the days of weapons testing, typical pinholes were about 1 m in length and weighed roughly 70 kg. The diameters of the pinholes were typically 0.25 mm, and the fields of view were typically 5 cm. Capturing neutron images of capsules used in ICF experiments requires a pinhole that is roughly 20 cm in length with a diameter approaching 20 μm and a field of view of about 500 μm. These dimensions push the limits of pinhole fabrication and fielding. The resulting images, however, provide powerful tools for the study of ICF capsule design. During 2003, new milestones in fabricating neutron-pinhole assemblies were met; as a result, the highest-resolution images recorded to date have been achieved along with recording the first "double-aperture" image using the Omega laser at LLE (University of Rochester). Data collected from these experiments were used to understand models of the dynamics of DT fuel and capsule-shell "mix." Understanding mix is critical not only for the design of ICF capsules and the environment necessary to achieve ignition at NIF but also for insight into the dynamics and performance of nuclear weapons.

Figure 3. Shot 31184 taken on April 1, 2003, with the Omega laser. Figure 3(a) is the color-coded intensity distribution of neutrons from the source as seen by both the high- and low-resolution pinholes. The red portion represents the high-fluence region, whereas the blue represents the low-fluence region. Figure 3(b) is the intensity profile of the red line drawn through the Figure 3(a).

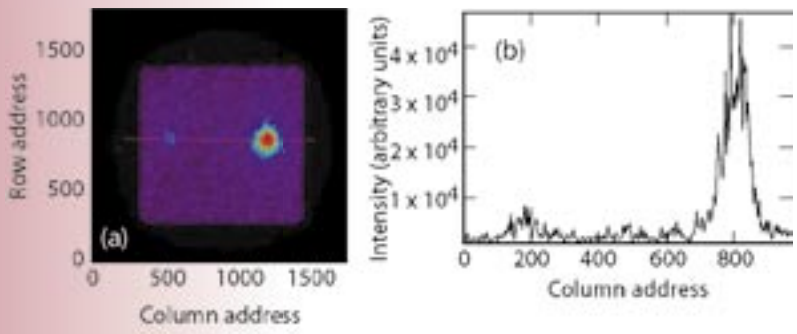

Pinhole Design and Fabrication

In a light-imaging pinhole system, the ideal pinhole is a perfectly opaque, infinitesimally thin, infinite plane that is pierced by an aperture, assumed circular for practical purposes. The source plane resolution of the pinhole image is determined by the aperture diameter and image magnification, whereas the field of view is infinite in extent. With penetrating radiation, the plane must be replaced with a plate of finite thickness to provide suitable opacity. As a consequence, the aperture becomes a three-dimensional profile through the plate. Thus, the field of view is no longer infinite but is determined by the geometry of the aperture profile. Along with this, the previous use of the two-dimensional aperture diameter to define the source plane resolution is modified to that of an "effective diameter." For the work done here, the effective diameter is defined as the radial distance from the pinhole axis at which paraxial neutrons have a probability of one-half of interacting. For a pinhole profile constructed from a double conic profile (i.e., intersecting left- and right-handed, right circular cones), a simple approximation to the source plane resolution is given by:

where λ is the mean-free path of the radiation in the material, θ is the opening angle of the cone sections,

$$\delta_{pin} = (\lambda \cdot \tan\theta \cdot \ln 2 + D_{clr})\left(1 + \frac{1}{M}\right) \qquad (1)$$

D_{clr} is the clear diameter of the pinhole, and M is the magnification of the system (i.e., the ratio of the image distance to object distance). For typical ICF experiments, M is large, O(100), and therefore the last factor may be ignored, and thus the source plane resolution is equal to the effective diameter.

In the experiments discussed here, a pinhole system capable of imaging 100-μm-diam objects with a spatial resolution approaching 15 μm was used. Figure 1b shows a schematic of the pinhole assembly designed with these specifications. The assembly was fabricated by precision machining two groves into two halves of a pair of matched tungsten plates, each plated with approximately 500 μm of gold. The mean-free path of 14-MeV neutrons in gold is approximately 3 cm. The tungsten provides rigidity, whereas the gold can be machined with diamond tools. The gold on each plate was first flattened with a large-radius (125 μm) tool. After the plate was locked in a horizontal position, grooves were machined into it using a 5-μm-radius, 90° diamond tool. The precision lathe used for this work has three orthogonal axes, each controlled to an accuracy of 0.025 μm. This accuracy allowed the two grooves in each plate to be precision cut into the gold. The plates were then aligned and mated together to create two pinholes within the assembly, 20 cm long. The two pinholes were designed to image an object in both apertures at a distance of 21 cm from the center of the assembly. For 14-MeV neutrons, the effective diameters of the two pinholes were roughly 22 and 52 μm with corresponding fields of view of about 400 and 600 μm, respectively.

Figure 2 shows how the pinhole assembly was deployed. The image shows the inside of the target chamber at the Omega laser. Various diagnostics, including the neutron-pinhole assembly, can be seen protruding from the chamber wall. The face of the pinhole assembly is placed 11 cm from

the center of the chamber and points toward the capsule position with an accuracy of 250 μrad. The bright spot in the center is the light produced from the implosion on shot 31184. The scintillator is placed 1,300 cm from the chamber center along the axis of the pinhole assembly. Figure 3 shows the relative intensity of neutrons interacting in the scintillator for this shot. The image is a magnified representation of the 14-MeV neutron source produced by the imploded DT capsule, blurred by the finite resolution of the pinhole imaging technique. The capsule was filled with 5 atm of equal (atomic) quantities of deuterium and tritium and imploded with approximately 23 kJ of energy from 60 beams. The total yield from the shot was 4×10^{13} neutrons. Figure 3(a) is the color-coded x-y intensity distribution showing the relative fluence of 14-MeV neutrons. The red area represents the region of higher-fluence regions, whereas the blue represents the lower-fluence regions. Figure 3(b) is the intensity profile of the red line shown in Figure 3(a). The line profile shows a clear indication of neutrons from both pinholes. The intensity from the small pinhole is less—that is, relative to the larger pinhole intensity—by the ratio of the effective pinhole areas, but the improved resolution of the small pinhole may be used in a complementary fashion to provide added information in the reconstruction of the image.

Asymmetric Direct Drive and Mix Physics

Using data such as those shown in Figure 3, it is possible to study phenomena important to the design of ICF capsules, in particular, the dynamics of fuel and capsule-shell mix. Historically, implosion simulations over-predict fusion-neutron yields from ICF capsules. The discrepancy is thought to occur by enhanced radiation and dilution of the fuel concentration at the fuel-shell interface due to mixing of these elements. During FY 2002 and 2003, these dynamics were studied by comparing neutron and x-ray images of ICF implosions with those predicted by a multi-fluid interpenetration model developed by Scannapieco and Cheng.[5] The model developed by Scannepieco and Cheng is attractive because it derives a set of multi-fluid moment equations from first principles while introducing only one free parameter. Further, this free parameter can be related to the collisional frequency of the system, which moves the approximations used to constrain the system from the governing equation level to the characteristic quantity for binary collisions.[5] During the experimental campaign, data from both symmetric and asymmetric implosions were collected and compared with the model. Applying the interpenetration model to an ICF capsule results in an equation of motion given by

where the collisional-drag frequency, ν_{ij}, is given by

$$\rho \frac{d}{dt}\left(\frac{\rho_i}{\rho}(u_i - u)\right) + \Sigma_j \frac{\rho_i \rho_j}{\rho} \nu_{ij}(u_i - u_j) = -\rho_i(u_i - u)\cdot\nabla u - \nabla \cdot P_i + \frac{\rho_i}{\rho}\nabla \cdot P \quad (2)$$

the following formula:

$$\nu_{ij} = \frac{C_j}{\Lambda + \alpha \int |u_i - u_j| dt}. \quad (3)$$

The parameter α is the experimentally determined quantity referred to above and represents the ratio of the mixing length to the thickness of the mix layer. The term Λ is the collision mean-free path.[6,7] The work in Reference 4 suggests that different modes of mixing are characterized by different values of α. These different modes include planar mixing or various types of jet mixing in stagnant surroundings. Figures 4 and 5 show the comparison between neutron images of prolate- and oblate-capsule shots along with simulated images where the parameter α is varied. As can be seen from these images, as α is increased (which corresponds to increasing the amount of mix), the size of the burn region decreases (which more closely models the experimental results). Figures 6 and 7 summarize the dependence of neutron yield on asymmetry. The interpenetration model predictions of this dependence as α is varied are overlaid on these two figures. The results of these comparisons (and of others that are not shown here) indicate a value of α = 0.07 +/– 0.01, which models the data well for capsules filled with DT at pressures of 2.5, 5, and 10 atm.

Conclusion

A number of conclusions have been drawn from these experiments. First, the results indicate that neutron production from DT fusion appears to be insensitive to the level of asymmetry being induced. Further, the interpenetration model of Scannapieco and Cheng[1] appear to predict this insensitivity with a single value of the parameter α at a number of different fuel pressures. Finally, it appears that a single mix parameter can be used to model symmetric and asymmetric implosions. These results provide solid constraints that hydrodynamic and "mix" modelers can use to advance the capability of codes applied to the design of ICF capsules and other relevant physics experiments.

The goal of the ICF research community is to achieve "ignition" of an ICF capsule at some point in the future. To achieve this goal, a tremendous effort must be expended to understand many of the impediments—not the least of which is the physics of capsule implosion, which, in turn, depends on

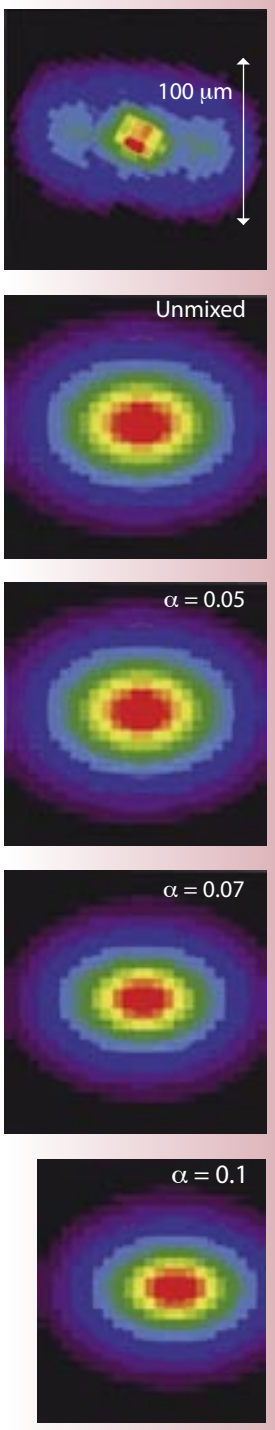

Figure 4. Comparison of shot 26665, a prolate implosion, and simulations using the model from Reference 1. By increasing the amount of mix (i.e. increasing α), the data are more closely modeled.

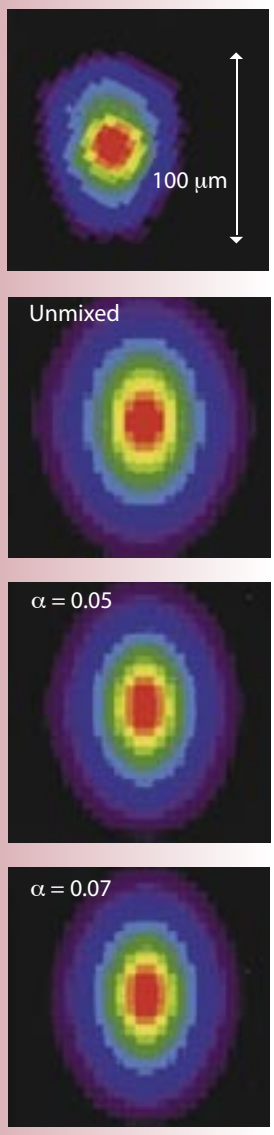

Figure 5. Comparison of shot 26666, an oblate implosion, and simulations using the model from Reference 1. As in Figure 4, the increasing amount of mix better models the size of the nuclear burn region.

the dynamics of mix. Neutron-imaging-diagnostics development and deployment in ICF experiments have played, and will continue to play, a critical role in understanding mix and other phenomena in ICF target design as the march towards ignition progresses.

References

1. D. Ress *et al.*, "Neutron imaging of inertial confinement fusion targets at Nova," *Review of Scientific Instruments* **59**, 1694 (1988).
2. J.-P. Garconnet *et al.*, "Neutron penumbral imaging of inertial confinement fusion targets," *Laser and Particle Beams* **12**, 563 (1994).
3. G.L. Morgan *et al.*, "Development of a neutron imaging diagnostic for inertial confinement fusion experiments," *Review of Scientific Instruments* **72**, 865 (2001).
4. C.R. Christensen *et al.*, "First Results of pinhole neutron imaging for inertial confinement fusion," *Review of Scientific Instruments* **74**, 2690 (2003).
5. A.J. Scannapieco and B. Cheng, "A multifluid interpenetration mix model," *Physics Letters A* **299**, 49 (2002).
6. S.I. Braginkskii, *Reviews of Plasma Physics* **1** (1965).
7. L. Spitzer, *Physics of Fully Ionized Gases* (Intersciences Publishers, New York, 1962).
8. B.E. Launder and D.B. Spalding, *Mathematical Models of Turbulence* (Academic Press, London, 1972).

Acknowledgment

To accomplish the work discussed herein required a significant effort on the part of individuals not listed above. In particular, we owe a debt of gratitude to the MST-7 team that fabricated the pinhole assembly, particularly Jacob Bartos and Felix Garcia, along with the target fabrication teams at both LANL and General Atomic. We would also like to thank Peter Ebey of ESA-TSE for ensuring there were DT targets available and Nick King of P-23 for the development of our camera and scintillating system. Finally, the data would not exist without the staff at the LLE, whose skillful operation of the Omega laser made this possible. In particular, we would like to thank William (Jack) Armstrong of LLE for his technical support and effort. This work was supported by DOE Contract No. W-7405-ENG-36.

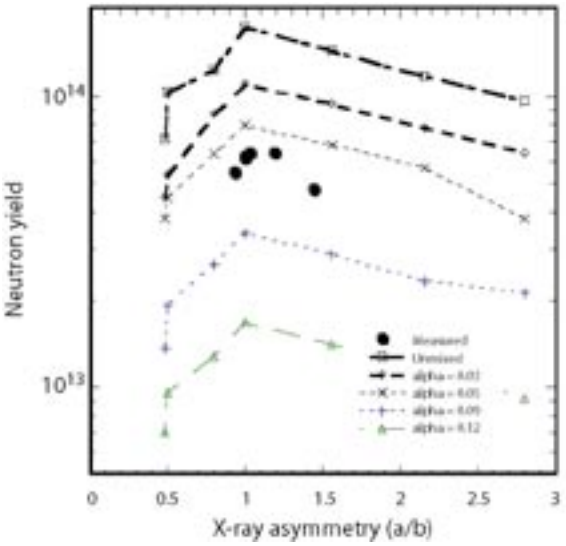

Figure 6. Comparison between data and simulation (as the amount of mix is varied) of neutron yield as a function of the asymmetry at capsule fills of 5 atm. The vertical axis is the yield in total neutrons, whereas the horizontal axis is the degree of asymmetry as measured from x-ray images. In the case of the model predictions, the x-ray images are simulated as well.

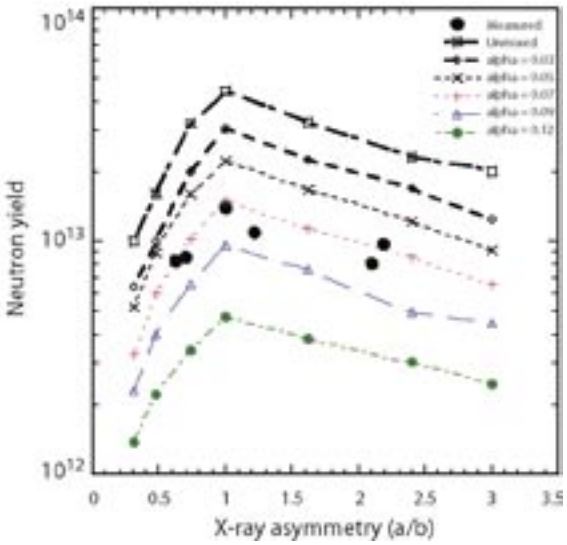

Figure 7. Same as Figure 6 but for 2.5-atm capsule fills.

For more information, contact Gary Grim at 505-667-8985, gpgrim@lanl.gov.

"Magnetic Reconnection" Studies Conducted at Los Alamos National Laboratory

T.P. Intrator, I.G. Furno, S.C. Hsu, E.W. Hemsing (P-24), G.M. Lapenta, P. Ricci (T-15)

Most of the known universe (about 99%) is composed of plasma, which is an ionized gas. Although ions and electrons are not joined as atoms and molecules, each can flow in fluid patterns. This state not only contains eddies, flow fields, waves, and shocks but also electric and magnetic fields. Some of the most interesting questions regarding the structure and dynamics of our universe involve this coexistence of flows and fields. A structure that generates magnetic fields from conductive-fluid flow is called a *dynamo*, and the annihilation of a magnetic field is called *magnetic reconnection*. When reconnection occurs, the magnetic-field energy is transferred to the plasma. Our research is focused on *magnetic reconnection* and is part of a larger P Division effort to establish a plasma-astrophysics presence in the world scientific community. Our research connects to LANL missions, including the physics of plasma devices for magnetic-fusion research, space "weather," satellite communications, and ASCI computing.

During five decades of study, researchers have largely regarded magnetic reconnection as a "black-box" process that begins with the dissipation of magnetic-field energy and ends in plasma-particle acceleration and/or thermal heating. Indeed, the slow build up of magnetic energy followed by an explosion that converts it into particle energy is almost always present in any magnetized plasma.[1,2,3] These dynamic explosions release energy anisotropically, whereby slow flows occurring in one direction can elicit large accelerations in another. In nature, these fast time scales can be orders of magnitude quicker than expected resistive diffusion times.

A detailed understanding of the magnetic-reconnection process has only recently started to emerge. Understanding this process could help researchers improve the control and confinement of magnetic-fusion plasmas and understand the stability and magnetic structure of magnetic-fusion-confinement devices. Moreover, long-standing solar-physics questions involving the origins of coronal heating, coronal mass ejections, and other coronal-magnetic activity might finally be solved. Accurate predictions of geomagnetic disturbances could be made, and the effect of solar wind interactions with the earth's magnetosphere on spacecraft environments could

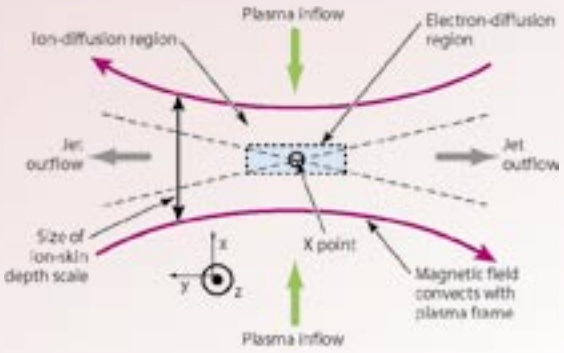

Figure 1. Schematic showing the reconnection plane, including slow plasma inflow velocity in the vertical direction. Anti-parallel magnetic fields convect inwards through a region of ion-skin-depth dimension. On the smaller electron-skin-depth scale (dashed box), a diffusion region containing electron microphysics determines the reconnection process. These two spatial scales have never been observed together in the laboratory. Note the similarity between this figure and Figures 3 and 4. The X point would occur if the size of the reconnection region were vanishingly small.

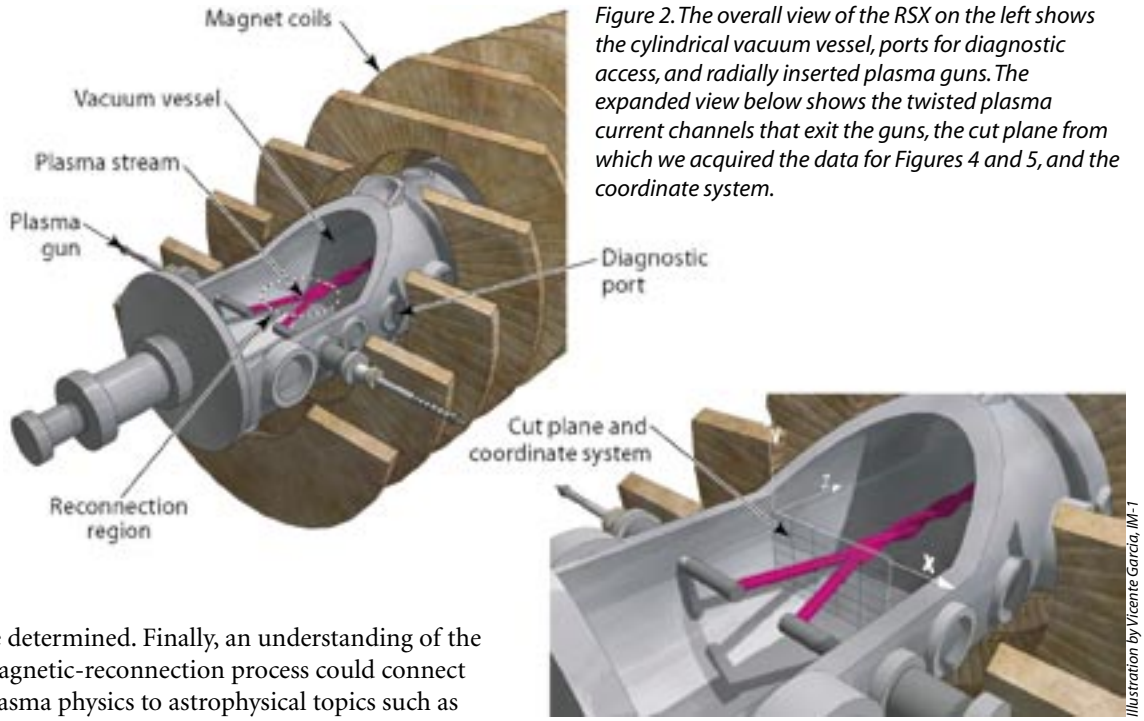

Figure 2. The overall view of the RSX on the left shows the cylindrical vacuum vessel, ports for diagnostic access, and radially inserted plasma guns. The expanded view below shows the twisted plasma current channels that exit the guns, the cut plane from which we acquired the data for Figures 4 and 5, and the coordinate system.

Illustration by Vicente García, IM-1

be determined. Finally, an understanding of the magnetic-reconnection process could connect plasma physics to astrophysical topics such as accretion disks; jet, star, and galaxy formation; and cosmic-ray acceleration—topics that had traditionally been studied only from the perspective of hydrodynamics, general relativity, and atomic physics.

Frozen-Flux Concept and Reconnection

Plasmas can be very good electrical conductors. Electric and magnetic fields cannot penetrate or *diffuse* into perfect conductors because induced eddy currents cancel out these fields. Conversely, fields that are "stuck" inside conductors take a long time to *diffuse* out (i.e., the magnetic flux is *frozen* into the moving plasma). Current flows much more easily along a field than across it, so magnetic field lines can be imagined as conducting wires that move with the plasma. During this process, oppositely directed field lines can be convected toward each other by fluid flow (e.g., the inflow region in Figure 1). Between the oppositely directed fields, there is a magnetically neutral line (*current sheet*) across which there is a reversal of the magnetic field. Diffusion occurs in that region, and the *frozen-in* condition of ideal magnetohydrodynamics (MHD) is broken. The magnetic fields can diffuse through the plasma, allowing the annihilation of oppositely directed magnetic field lines and forcing the lines going in one direction to connect to the ones going in the opposite direction. These "reconnected" field lines act as rubber bands under tension and pull away horizontally from the diffusion region. Consequently, plasmas are flung as if by a slingshot, which could explain many impulsive phenomena.

Microphysics of Fast Reconnection

At present, a major debate exists regarding the microphysics that influence a fast reconnection rate. This topic has been considered theoretically from two distinct perspectives beyond the scope of resistive MHD. "Anomalous" micro-instability-induced resistivity [which in the collisionless limit can be orders of magnitude larger than the classical (Spitzer) resistivity] can be invoked to explain enhanced dissipation rates inside the reconnection layer. On the other hand, neglected terms of the two-fluid generalized Ohm's law (i.e., the electron momentum equation) can become important on spatial scales smaller than the ion-skin depth c/ω_{pi}, where c is the speed of light, and $\omega_{pi}(\omega_{pe})$ is the ion (electron) plasma frequency.[4] A key experimentally testable feature of the two-fluid reconnection theory is the expected development of a reconnection layer with a two-scale spatial structure. This feature arises because ion and electron motion decouple in between ion and electron c/ω_{pe} skin-depth length scales. With its scalability in collisionality and magnetic fields, the Reconnection Scaling

Experiment (RSX), which is currently under way at LANL, should allow us to address this question and/or observe signatures of the electron layer. We can independently scale plasma density (and thus the collision frequency), and we can scale the axial magnetic field to change the ion gyro radius.

We are exploring magnetic reconnection in the RSX. Two parallel current plasma channels are produced using plasma guns. Most other experiments are toroidal, but this one has a simpler linear geometry. The RSX cylindrical vacuum chamber has many ports for easy placement of diagnostics and plasma guns (Figure 2). The overall view shows a cutaway schematic of two current channels created by two plasma guns, which are inserted radially into the vacuum chamber. A set of external coils generates the axial guide field B_Z. The expanded view shows the helical twisting and merging of these current channels. The coordinate-system axes are indicated for a cut plane through this interaction region. Typically in RSX, we generate hydrogen plasmas with a large Lundquist number ($S > 100$), current densities of $J < 1$ MA/m^2, and electron densities and temperatures in the range of $n_e \sim 1$ to 30 x 10^{13} cm^{-3} and $T_e \sim 10$ to 20 eV, respectively. One major advantage of the plasma-gun technology is that no complicated startup scheme or evolution to equilibrium is required. It also allows a high degree of flexibility in scaling the source characteristics independently of the different parameters important in the reconnection process.[4,5] Because the plasma guns create the plasma, both the collisionality (density) and the magnetic-field component, normal to the reconnection layer (current density), can be controlled independently of the plasma-formation process.

Data from RSX

We completed measurements of the magnetic structure in a two-dimensional cut plane (Figures 2 and 3). Figure 3 shows the magnetic topology and diffusion region from the cut plane in Figure 2. Magnetic probes inserted into the plasma gave us a time history at each point, and we explored the full plane over many repetitive shots. An example of vector data (B_x, B_y) in the x-y plane for a time late in the evolution of the reconnection layer is shown in Figure 4. The diffusion region is indicated by the dashed circle, where a jump in B_x is apparent on a vertical cut at x = 0.280 m. These data were taken using a large-guide magnetic field of $B_{0z} = 400$ Gauss. This magnetic field was large enough to magnetize the ions even in the diffusion region where the B_x field vanishes and to maintain a very small beta [$\beta = nT/(B^2/2\mu_0) << 1$, which is the ratio of particle pressure to magnetic pressure]. A sketch of the B_x time history for this vertical cut is shown in Figure 5. Four selected times show how the jump in magnetic field increases with time. Interestingly, the scale size of this diffusion layer is approximately 0.5 cm. This scale size is far smaller than the ion-skin depth (≈ 7 cm) and not too

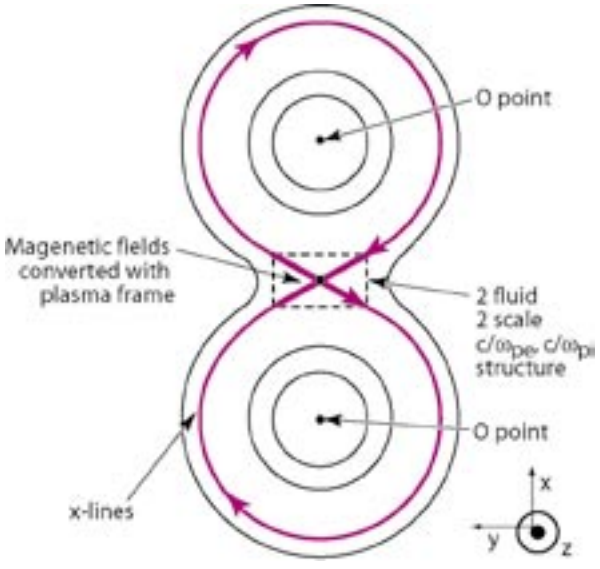

Figure 3. The O points locate the center of each current channel; an X point is located in the diffusion region, which is indicated by dashed lines. The x-y plane corresponds to Figures 1, 3, and 4.

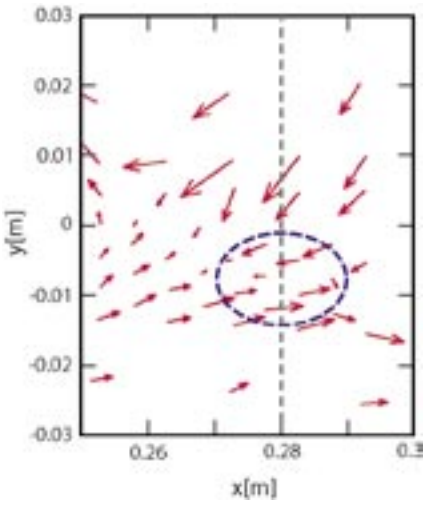

Figure 4. Vector data (B_x, B_y) in the x-y plane. Note the reversal in B_x across the neutral sheet region (dashed circle).

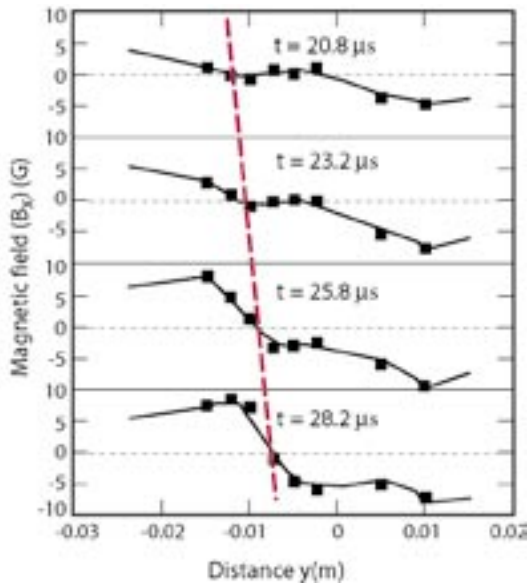

Figure 5. Magnetic field B_x on a vertical cut at y = 0.28 m. Note how the jump in B_x becomes steep as time progresses for each time indicated on each panel of the figure.

different from the electron-skin depth (≈ 0.2 cm) and the ion gyro radius (0.8 cm). In the near future, we will scan the effects of the externally applied guide field. However, this is at least one example where the size of the diffusion region is quite different from the ion-skin depth predicted by the usual reconnection theories.

Conclusion

Most of the known universe is plasma, and reconnection is ubiquitous in much of it. Magnetic reconnection is thought to convert magnetic-field energy into particle, beam, and thermal energy. The debate concerning the microphysics of reconnection includes predictions that the scale length for the neutral current sheet is the ion-skin depth. Nevertheless, we show here one counter example, using data from RSX at large-guide magnetic field. We intend to investigate the scaling of these results.

References

1. D. Biskamp, "Collisional and collisionless magnetic reconnection," *Physics of Plasmas* **4,** 1964 (1997).
2. J.F. Drake, "Magnetic explosions in space," *Nature* **410**, 525 (2001).
3. J. Glanz, "Unlocking secrets of magnetic fields' power," *New York Times*, October 24, 2000.
4. M. Shay, J. Drake, R. Denton, and D. Biskamp, "Structure of the dissipation region during collisionless magnetic reconnection," *Journal of Geophysical Research* **103**, 9165 (1998).
5. I.G. Furno, T.P. Intrator, E. Torbert *et al.*, "Reconnection scaling experiment: A new device for three-dimensional magnetic reconnection studies," *Review of Scientific Instruments* **74**, 2324 (2003).

Acknowledgment

The RSX is a collaborative effort between P Division and T Division at LANL and is sponsored by LANL LDRD funding.

For more information, contact Thomas Intrator at 505-665-2927, intrator@lanl.gov.

Radiological, Chemical, and Biological Decontamination Using Atmospheric-Pressure Plasmas

L.A. Rosocha, J. Park (P-24), J.R. FitzPatrick (C-AAC), H.W. Herrmann (on entrepreneurial leave to APJeT, Inc.)

Researchers at LANL have applied a technology known as the atmospheric-pressure plasma jet (APPJ) to the decontamination of radiological, chemical, and biological agents from surfaces. [This unique technology (Figure 1) was invented at LANL in 1995[1] and won an R&D 100 Award in 1999.] An APPJ[2,3] produces a gas stream of highly reactive chemical species identical to those currently used by the semiconductor industry to clean silicon wafers. The APPJ reactor, however, creates non-thermal plasmas that can clean surfaces in "open air" instead of in vacuum. [The electrons, ions, and neutral-gas species that make up non-thermal plasmas are not in thermal equilibrium. The electrons are energetic ("hot"), whereas ions and neutral gases are near ambient temperature ("cool")]. The open-air concept eliminates the cost, time, and effort previously required to plasma-process work pieces in special vacuum chambers and, as a result, opens up a host of new plasma-processing applications. Although the effluent of the APPJ (Figure 1b) may appear somewhat like the flame of a Bunsen burner, its temperature can be maintained cooler than that of a hair dryer's exhaust. Chemically reactive species of oxygen generated by an APPJ device essentially "burn" many organic materials, such as oil and grease, from surfaces at these relatively low temperatures.

APPJ technology is used in a number of industrial and military applications. In materials processing, for example, applications range from etching silicon wafers to modifying surfaces to increase their wettability or absorption. Applications involving chemical and decontamination processing include the destruction of chemical and biological warfare (CBW) agents and the removal of radionuclides from surfaces and equipment. The development of this unique technology spans the regimes of bench-top studies to prototype demonstrations.

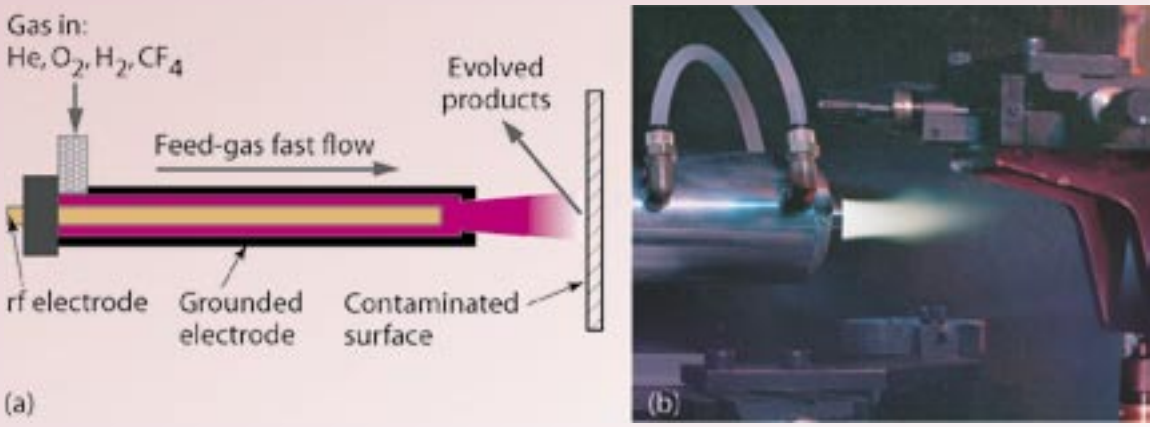

Figure 1. (a) Schematic of an rf-driven APPJ. (b) Photo of the APPJ device in operation.

Atmospheric-Pressure Plasma Jet

The APPJ produces a non-thermal, glow-discharge plasma operating at atmospheric pressure. The discharge uses a feed gas consisting primarily of an inert carrier gas, such as helium, and a small amount of an additive (e.g., O_2) that is activated. The feed gas flows between an outer, grounded, cylindrical electrode and an inner, coaxial electrode powered at an rf of 13.56 MHz (Figure 1a). The electric field produced between the electrodes causes the gas to breakdown into a "plasma state," or an ionized gas capable of conducting electricity. While passing through the plasma, the feed gas becomes excited, dissociated, or ionized by interacting with energetic electrons. Once the gas exits the discharge volume, ions and electrons are rapidly lost via a process known as recombination. Metastable species and radicals are left behind. Oxygen-containing plasmas, for example, produce reactive oxygen species, such as metastable oxygen (O_2^*), atomic oxygen (O), and oxygen ions (O_2^+). These reactive species tend to live relatively longer than electrons and ions and readily oxidize, or combust, many organic compounds on surfaces, including oil and grease.

Plasma feed gases can easily be tuned to produce tailor-made chemistry. For instance, hydrogen can be added in place of O_2 to produce a reducing environment of atomic hydrogen. CO_2 can be used in place of O_2 to minimize the amount of generally unwanted ozone (O_3), which tends to form downstream of an oxygen discharge. Reactive species can be directed onto a contaminated surface at high velocity where they can selectively neutralize organic materials without damaging the underlying surface. The temperature of this gas discharge typically ranges from 50°C to 300°C, which allows for plasma processing of sensitive materials and equipment at low temperatures and accelerated processing of more robust surfaces at higher temperatures.

"Polishing" Actinide-Contaminated DynEx Vessel Surfaces

Members of P-24, in collaboration with the Actinide Analytical Chemistry Group of the Chemistry Division at LANL, are conducting an Environmental Management Science Program (EMSP) to demonstrate general-purpose decontamination of superficial actinide contamination. The EMSP provides the science base for the APPJ application.

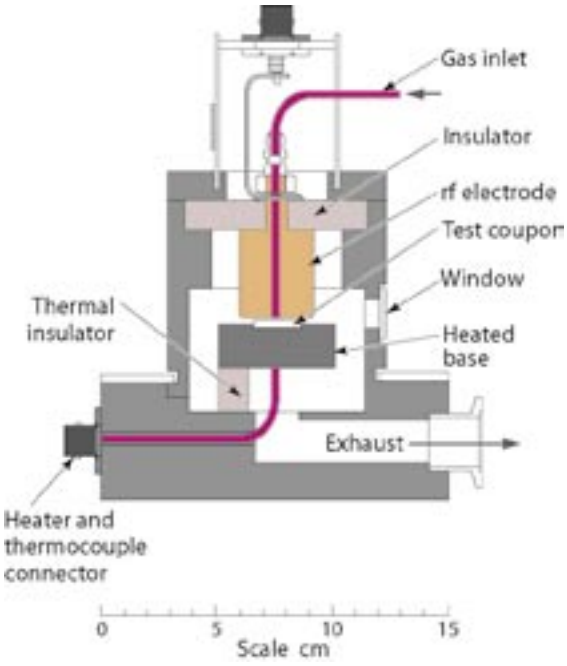

Figure 2. Schematic of the APPJ device used for actinide- and surrogate-actinide-etching studies.

In addition to this general decontamination project, we are investigating APPJ technology as a means to fully satisfy the special needs of the DynEx program in a cost-effective manner. DynEx studies are a required capability for the nuclear weapons program in general and for stockpile stewardship and weapons and weapons-component certification. These studies also provide data essential for the analysis and understanding of weapons-performance issues.

The current technology used for surface decontamination of residual waste from plutonium-processing operations (gloveboxes, tools, pipes, etc.) involves an acid-wash process that generates many liters of mixed-hazardous waste per unit. Moreover, this process requires nearly 8 hours of manual labor and results in considerable personnel radiation exposure. APPJ-plasma processing provides a convenient and waste-free method for decontaminating surfaces and recovering residual quantities of actinides (e.g., plutonium, uranium) that form volatile fluorides. In this method, a plasma generates a reactive chemical "intermediate" (e.g., fluorine atoms) from an inert feed gas (CF_4 or NF_3). This intermediate reacts with an actinide-contaminated surface to form a volatile gaseous product that is then pumped off the surface, leaving

it clean and decontaminated. The off-gas from this procedure is sent through a filtration system that traps and recovers any residual product. Known as "Atmospheric Pressure Decontamination (APD) DynEx Vessel Polishing," the goal of this DOE Defense Programs project is to determine whether the APPJ technology can decontaminate plutonium and uranium from metal surfaces, like actinide-contaminated DynEx vessels, in a *dry, safe* manner.

In APD-etching studies, 1/8-in.-thick, 1-in.-diam stainless steel coupons (disks) were impregnated with small amounts of plutonium and uranium and then exposed to an APPJ effluent. The APPJ device (similar to the one shown in Figure 2) contains a coupon holder and a stage for heating the coupons. The APPJ and associated enclosure are placed inside a glovebox at the Chemistry and Metallurgical Research Facility at LANL. The APPJ was operated at 700 W. About 90% of the uranium was removed in 10 minutes, whereas about 50% of the plutonium was removed in the same amount of time. The plutonium-doped coupons were further exposed at 10-minute intervals (Figure 3). We have also used *surrogate* actinide materials, such as tantalum and tungsten, in etching studies to safely test and evaluate the APPJ technique without the handling hazards and safeguards associated with actinide materials. In these studies, small quantities of NF_3, CF_4/O_2, or SF_6 were added to the primary helium feed gas to produce chemically active atomic fluorine. Using the APPJ method, removal of the actinide surrogate, tantalum, was demonstrated at > 10 μm per minute.

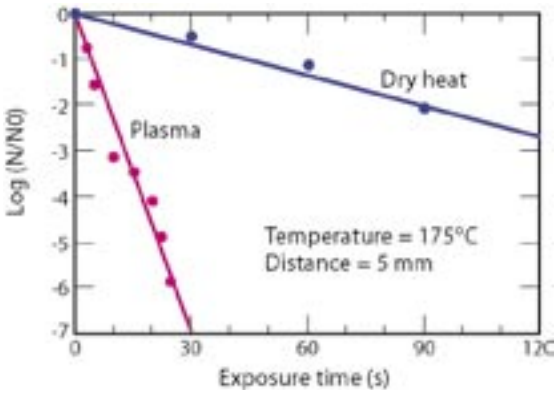

Figure 4. Destruction of the Anthrax surrogate BG using the APPJ method as compared to the dry-heat treatment.

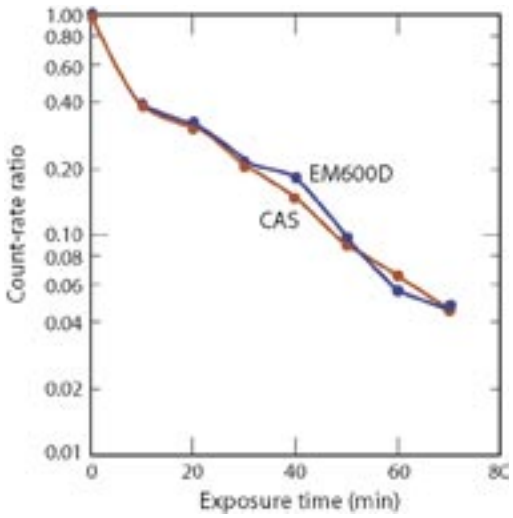

Figure 3. Removal data for plasma processing of plutonium-doped disks (ratio of counts at a given exposure time to counts with no exposure, i.e., initial activity).[4] CAS is an acronym for Canberra Alpha Spectrometer, and EM600D is the Eberline radiation monitor.

Chemical and Biological Weapons Decontamination

Events that happened in the U.S. after September 11, 2001, confirmed that chemical and/or biological agents could be used to inflict terror on civilians and to damage the infrastructure of our nation. Technology is therefore needed not only to detect these horrific weapons but also to reclaim and restore normal activities by decontaminating the areas targeted by CBWs. The P-24 CBW program at LANL is focused on the development of an all-dry, decontamination APPJ process suitable for use on sensitive equipment, such as computers, industrial machinery, and communications centers. As such, the "downstream" APPJ system developed for this program is portable, inexpensive, spot-specific for treatment, and amenable for use with objects of any size. It was used in tests to destroy biological- and chemical-warfare-agent surrogates, as well as actual chemical-warfare agents.[5] Active species produced inside the APPJ are rapidly blown out of the source and impinge a target surface 2 to 10 mm downstream. Most often, a He/O_2 feed gas is used, which produces a mix of atomic oxygen, metastable molecular oxygen, and small amounts of ozone. Figure 4 shows the results for decontamination of Bacillius globigii (BG), a surrogate for Anthrax spores, for both plasma and dry-heat treatments.

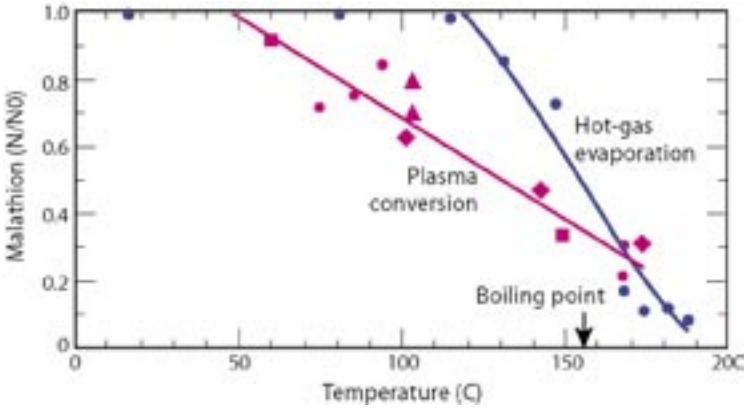

Figure 5. Destruction of the chemical-warfare surrogate, Malathion, using the APPJ method as compared to the dry-heat treatment. (Note: the plasma case has multiple symbols, representing more than one experiment.)

(The dry-heat treatment blows hot air, or some other gas, onto the biological agent.) Results indicate a seven-log kill (i.e., a factor of 10 million removal or decrease of the contaminate) of BG spores in 30 s with an APPJ effluent temperature of 175°C—which is ten times faster than dry heat at the same temperature! The APPJ also decontaminated surrogates for sulfur mustard and VX nerve agent and for actual VX. Figure 5 shows the results for the decontamination of Malathion (a pesticide surrogate for the chemical-warfare agent VX) for the plasma and dry-heat treatments.

Conclusion

In the near future, we will carry out parametric studies to determine the effect of gas mixture, coupon temperature, power, and gas-flow rates in an attempt to optimize the removal of plutonium and uranium from metal surfaces. If those studies indicate sufficient efficacy for the process, we will conduct scale-up studies to aid in the design of systems for decontaminating actual vessels or larger quantities of contaminated metals.

References

1. G.S. Selwyn, "Atmospheric pressure plasma jet," U.S. Patent 5-961-772, January 23, 1997.
2. A. Schütze, J.Y. Jeong, S.E. Babayan, J. Park, G.S. Selwyn, and R.F. Hicks, "The atmospheric-pressure plasma jet: A review and comparison to other plasma sources," *IEEE Transactions on Plasma Science* **26**, 1685 (1998).
3. J. Park, I. Henins, H.W. Herrmann, G.S. Selwyn, J.Y. Jeong, R.F. Hicks, D. Shim, and C.S. Chang, "An atmospheric-pressure plasma source," *Applied Physics Letter* **76**, 288 (2000).
4. L.A. Rosocha and J.R. FitzPatrick, "Recent results on actinide decontamination with an atmospheric-pressure plasma jet," Los Alamos National Laboratory report LA-UR-03-6689.
5. H.W. Herrmann, I. Henins, J. Park, and G.S. Selwyn, "Decontamination of chemical and biological warfare agents using an atmospheric-pressure plasma jet," *Physics of Plasmas* **6(5)**, 2284 (1999).

Acknowledgment

This work is a collaborative effort involving researchers from the P Division and the C Division and was sponsored by the DOE Environmental Management Science Program and Defense Programs.

For more information, contact Louis Rosocha at 505-667-8493, rosocha@lanl.gov.

Experimental Physics Using the Z Accelerator at Sandia National Laboratories

R.G. Watt, G. Idzorek (P-22), R.E. Chrien, D. Peterson (X-2)

The natural world is constantly attempting to reach an equilibrium state most simply thought of as a state in which quantities such as temperature or density are uniform throughout a volume. When quantities such as temperature vary from one point to the next in the volume, these differences can act to produce a force that tries to restore that quantity to a uniform state. These restoring forces can lead to familiar processes such as water being ejected from the end of a hose because of the pressure difference between the inside and the outside of the hose (a pressure gradient). The flow of heat down a bar of metal that has been heated on one end by a torch is another process (thermal diffusion) created by the difference in temperature from point to point along the bar (a thermal gradient). Forces resulting from gradients are less familiar than forces such as gravity, but they can be the driving engine in processes from the very small (mixing of two different liquors in a mixed drink or the rate of chemical reactions in a retort—both driven by concentration gradients) to the extremely large (mass ejection, astrophysical jet creation, and shock formation—all driven by energy density gradients in supernova explosions). While forces that result from gradients play a role in daily life, they can also play a dominant role in less mundane fields such as astrophysics and the physics involved in nuclear weapons.

Radiation Transport

The concept of a radiation temperature (T_{rad}) and of the transport of radiation through stellar systems arises from a logical extension of the familiar concepts discussed above (e.g., heat emission from a thermally warm object). These concepts extend from infrared radiation from a hot metal bar at a few 100 K all the way to x-rays emitted from an extremely hot object (e.g., a blackbody radiator) with an equivalent temperature in the million-degree range. Understanding radiation transport is important because it plays a prominent role in the evolution of stars and in the functioning of a nuclear weapon. Like thermal temperature gradients that cause the diffusion of heat down a metal bar, T_{rad} gradients cause the transport of radiation through systems. For example, radiation from a star is transported from the high T_{rad} region deep within the star where it was created out into the cold surrounding interstellar region. On its way out, the radiation moves through regions where various radiation-transport models may be valid—all driven by T_{rad} gradients. Transport processes in a star are the subjects of intense study using astrophysical simulations.

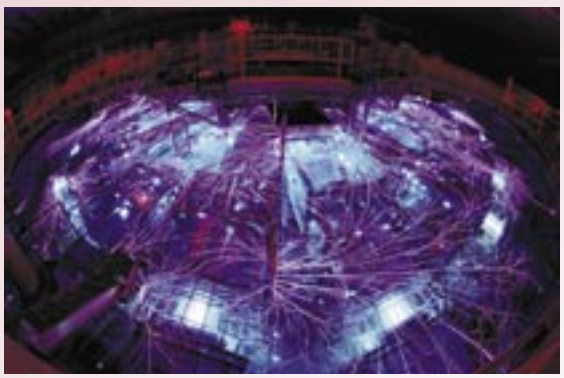

Figure 1. Bird's eye view of the Z accelerator as it fires.

The Z pulsed-power accelerator at SNL generates an environment in which large T_{rad} gradients exist at temperatures of about 2 x 10^6 K (220 eV). This extreme environment allows us to study the underlying physics behind radiation transport. Because of the importance of radiation transport, experimental data are needed to ensure that we have the correct physics understanding, models, and simulation tools. Data from experiments on Z can lead to new models or confirm existing models and thus validate LANL's physics and engineering simulations. Experimental tools like the Z accelerator are needed to produce radiation-transport data and other types of data, including material properties of metals (e.g., beryllium and uranium) of interest to the laboratory.

The Z Accelerator

The Z accelerator reuses the energy-storage system originally built for the ICF PBFAII project at SNL in the early 1980s. The Z accelerator is a high-energy capacitor bank comprised of 36 parallel modules arranged in a circular array. The 36 current pulses are coupled towards the center of the array through a series of pulse-forming networks (PFNs). These PFNs are used to compress the many microsecond current pulses into 100-ns current pulses. After penetrating the wall of a vacuum vessel, the 36 individual current pulses are combined into a single current pulse. This single pulse is then transported into the center of the chamber where it is converted into some form of energy used for an experimental physics study.

The capacitor banks, PFNs, vacuum vessel, and ancillary equipment reside in a several-story building designed for the task. Service utilities in the building provide vacuum, high-pressure air, normal air-conditioning service, and high-voltage service for charging the capacitor bank. Also, a high-capacity crane and a multitude of shielded enclosures (one belonging to P-22) service diagnostic instruments in the electrically hostile environment. The main control room is a shielded enclosure that protects the computer control system when Z fires.

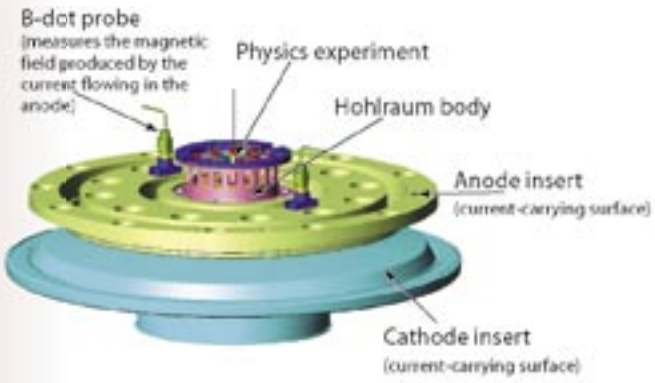

Figure 2. An anode and cathode insert with attached dynamic hohlraum body.

The high-power Z Beamlet Laser (ZBL) was recently constructed as a new capability in an adjacent building to the Z accelerator. (Parts from LLNL's beamlet laser system—the prototype for each arm of the NIF—were refurbished for the construction of ZBL.) The light from ZBL is transported into the Z target chamber through an optical transport system that spans the space between buildings. The ZBL light pulse produces x-rays from a metal foil in the Z vacuum vessel. The x-rays are produced next to a physics experiment at the center of the target chamber. They are typically used as an x-ray backlighter to illuminate the physics experiment and to take a dynamic image of its evolution in a manner similar in concept to DARHT and PHERMEX at LANL.

Figure 1 shows a bird's eye view of the Z accelerator as it is firing. (From the image, one can see why all electronics are generally located in shielded enclosures!) The lightning bolts in the image are above the PFNs. The PFNs reside in low-conductivity water where pulse duration compression from 10 μs to 100 ns takes place for subsequent injection into the target chamber. The discharges (lightning bolts) are due to energy leaking out of the high-voltage switches in series with the PFNs into the surrounding environment. From the water section, the pulse-forming lines feed through an insulating water-vacuum interface and onto a radial magnetically insulated transmission line (MITL), which then feeds the center of the machine where the physics experiment is conducted. Because of the total amount of energy involved (~ 14 MJ at 90 kV) in each discharge, the very center of the MITL has an interchangeable ~ 12-in.-diam insert that holds the physics experiment and the final disposable sections of the anode and cathode current conductors. This insert (Figure 2) is destroyed on each shot. The MITL must be removed and physically cleaned after each shot, which limits the facility to a single shot each day. In an x-ray production mode, Z is the most powerful x-ray source in the world (~ 250 TW in a 3–5 ns pulse) and provides an unmatched tool

for radiation driven experiments conducted by LANL and others. X-ray production, x-ray driven experiments, and other experimental uses of Z will be discussed below.

Radiation-Driven Experiments

For production of x-ray radiation, the electrical current flowing in the system is run through a set of very small diameter wires inside a confining structure, known as a hohlraum, which is used to contain any x-ray radiation that is produced from the experiment. The wires collapse toward the center of the vacuum vessel under the magnetic forces acting on them. The 12-in.-diam sacrificial insert (in the configuration shown in Figure 2) is comprised of a final anode and cathode section with a slotted dynamic hohlraum body mounted on top of the anode. Current delivered by the MITL travels radially inward on the cathode and up through a set of 360 tungsten wires, each ~ 10 μm in diameter, located inside the hohlraum body. The current then returns along the top and down the side of the hohlraum body and finally to the capacitor-bank modules via the anode and the MITL. In this configuration, magnetic forces drive the wires radially inward at high velocity until they stagnate near the axis. Their kinetic energy is converted into thermal energy, which radiates away in the form of x-rays that are absorbed and re-radiated inside the hohlraum body. The resultant x-ray flux is used to drive physics experiments either around the periphery of the hohlraum or on the top of it.

Copious amounts of thermal x-rays are produced when an array of wires collapses either onto themselves (as in a vacuum hohlraum, Figure 3) or onto a low-density foam located on the axis of hohlraum (as in a dynamic hohlraum). The vacuum hohlraum can generate an environment with an equivalent blackbody temperature of 145 eV inside a solid-wall hohlraum. The wall of the hohlraum can then be populated with multiple physics packages for studies of radiation flow inside closed geometries and flow through free-standing low-density foams and for studies of aperture closure driven by radiation and shocks that impinge on the gold hohlraum wall.

Alternatively, the dynamic hohlraum produces radiation from a wire array as it impacts upon a low-density foam located in the center of the array, subsequently thermalizing the kinetic energy in the wires and radiating the energy vertically. This radiation can be directed out of the top and bottom of the pinch to a physics experiment above or below the wire array, rather than around the periphery of the hohlraum body as in the case of a vacuum hohlraum. This process produces a much higher-radiation temperature (220 eV) to drive a single package located above the hohlraum for similar studies. A recent radiation-transport experiment that investigated radiation loss through the thin gold wall of a physics package located above the pinch using the ZBL system for backlit imaging is discussed in this report ("X-ray Diffusion through a Thin Gold Wall," page 84) P Division and SNL use vacuum hohlraums to study both weapons-physics issues and astrophysical jet formation and dynamic hohlraums to study both weapons-physics issues and indirect-drive ICF.

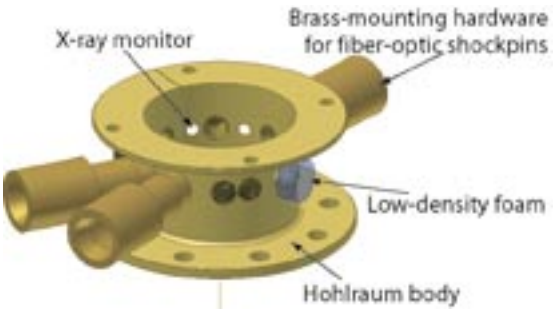

Figure 3. A typical experiment using a vacuum hohlraum with its outside wall populated by a number of experiments. This vacuum hohlraum shows four physics experiments located around the periphery of the hohlraum body. Three experiments are serviced by fiber-optic shock pins that are contained within massive radial structures (the brass-mounting hardware shown in the figure). There are also several apertures covered with foils and a low-density foam physics experiment to be radiographed by the ZBL system. The radiograph of the foam is taken as a radiation-driven shock passes radially through it.

Materials Experiments

For dynamic materials studies, the current is transmitted through the sample and then returned to the capacitor bank through a low-impedance circuit. The conductor wall is the material sample under study. The magnetic field generated between the central rod and the conductive sample can create a pressure in the sample (which is mounted on the return conductor wall) of up to 3.25 Mbar (in copper). This pressure can be used in shockless ICEs. When used in a flyer-plate mode for subsequent impact on material samples in past experiments, the Z accelerator has produced up to 28-km/s velocities in the flyer plate. In either event, the subsequent response of the material under study is used to accurately determine the equation of state of a material to ensure the integrity of simulations. P Division and DX Division use this configuration with the shock physics group at SNL to study many materials.

Several experiments conducted using the Z accelerator are discussed in detail in the project descriptions in this activity report.

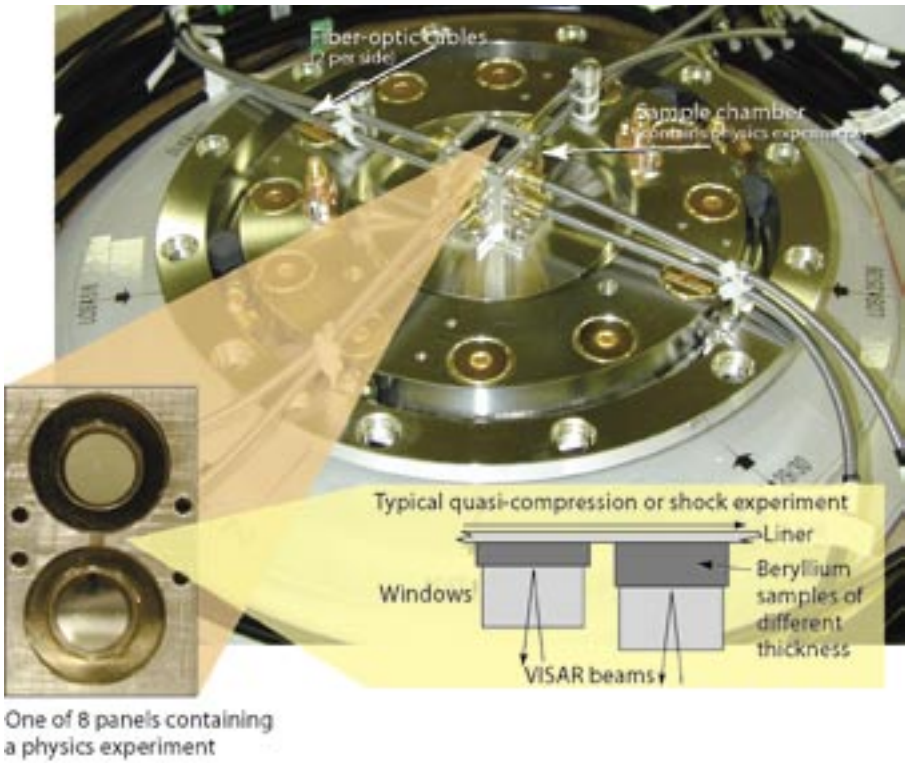

Figure 4. Four sample panels are arranged in a square pattern with each of the four panels having two samples under test. In the pictured experiment, beryllium samples are in intimate contact with the aluminum current-carrying conductor. The beryllium samples are subjected to quasi-isentropic compression. The particle velocity of the beryllium/window interface is recorded using VISAR. By conducting experiments with varying thicknesses of beryllium, we can determine a complete understanding of the isentrope of beryllium.

Acknowledgment

The researchers would like to acknowledge the MST-7 target-fabrication team for preparation of all physics experimental packages used in the Z experiments. We also wish to acknowledge the SNL Z Wire Array Laboratory and the Z Accelerator Load Assembly designers for the design and assembly of all radiation-producing wire-array systems. Finally, these types of experiments could not be performed without the input from a large number of colleagues in DX, P, and X Divisions at LANL during the planning of Z experiments. This work was sponsored by the Office of Secondaries and Inertial Fusion in DOE Defense Programs.

For more information, contact Robert Watt at 505-665-2310, watt_r@lanl.gov.

FRX-L: A Plasma Injector for Magnetized Target Fusion

G.A. Wurden, T.P. Intrator, J.M. Taccetti, S. Zhang, S.C. Hsu, Z. Wang, W. Waganaar, D.W. Begay (P-24), M.G. Tuszewski (NIS-2), C. Grabowski, J. Degnan, E. Ruden, B. Martinez (Air Force Research Laboratory)

Since the early 1950s, LANL has conducted research into ways to achieve controlled thermonuclear fusion to eventually create a new energy source[1] for the benefit of mankind. In the last decade, LANL has largely focused on collaborating with other experimenters around the world to build and diagnose the most advanced (and usually quite large) experimental fusion machines. In the background, several scientists and very small teams at LANL have been developing a new fusion concept that could lead to a faster, better, and cheaper approach to fusion energy.[2] This concept, generically called "magnetized target fusion" (MTF), lies somewhere in-between the more established approaches of magnetic fusion energy (MFE), which uses large magnetic bottles to confine hot plasma for long periods of time, and inertial fusion energy (IFE), which uses lasers or ion beams to implode tiny fuel capsules in a few nanoseconds.

A Different Approach to Generating Fusion Energy

MTF offers the possibility of achieving useful thermonuclear fusion conditions with a radically different approach—combining features of both MFE and IFE. MTF has the potential of operating at higher fuel density and of being more compact than MFE while at the same time alleviating the huge power requirements needed for IFE. As such, MTF will enable the use of slower (and therefore cheaper) pulsed power that has (literally) been around for decades. This innovative method basically begins with the production of an initial "warm" plasma embedded in a magnetic field (Figure 1). This plasma is then injected into an adjacent region where it is compressed to thermonuclear conditions using pulsed-power technology developed by the DOE Defense Programs to study materials under very high-pressure conditions. Defense Programs technology essentially "moves metal fast"—that is, a solid metal "liner" is imploded at extreme speeds. The region into which the MTF plasma is injected is surrounded by a thin aluminum cylindrical liner, which is then crushed in about 20 μs. The compression rapidly increases the magnetic field and the density and temperature of the plasma by a factor of 30 to 100, establishing thermonuclear conditions. As a result, the plasma should easily fuse and therefore release significant amounts of energy.

The ultimate goal of this research is to develop a fully operational pulsed-power fusion machine. The effort will combine 30 years of work at LANL to develop a class of plasmas called "compact tori," including one type, in particular, called the "field-reversed configuration" (FRC),[3] with 20 years of pulsed-power-technology development. To address this goal, we began an effort about four years ago to combine the required initial plasma and the liner implosion technology into a scientific effort that will hopefully lead to the first MTF physics demonstration.

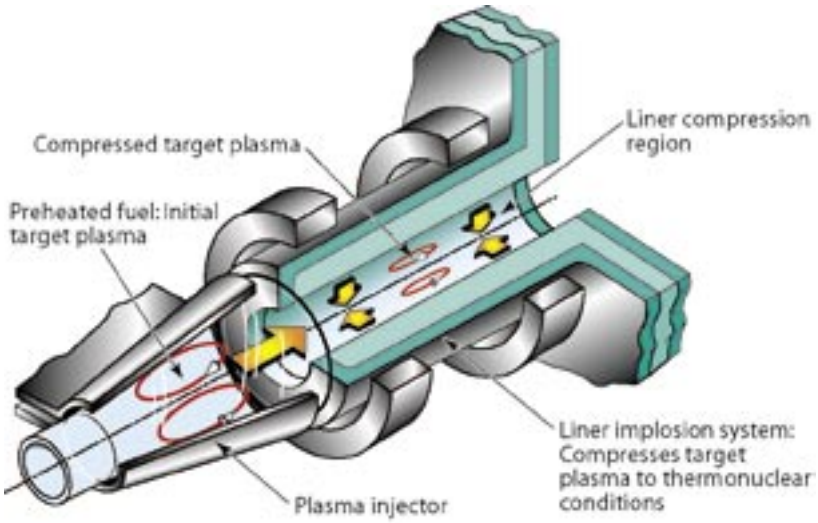

Figure 1. Rendering of MTF elements, including the initial target plasma, which is then injected into a liner compression region where the plasma can be compressed to thermonuclear conditions.

Efforts Toward a Field-Reversed Configuration Machine

The research program at LANL involves efforts (1) to demonstrate a suitable plasma injector, called the "FRX-L,"[4] where FRX refers to "field-reversed experiment," and the "L" refers to "liner," (2) to develop the "can crusher" at the Air Force Research Laboratory (AFRL) in Albuquerque, NM, and mate it to the plasma injector, and (3) to predict and model the plasma implosions using sophisticated computer codes with data from fast-plasma diagnostic tools. Other scientists at the University of Nevada, Reno; General Atomics; and LLNL are also conducting research into elements of MTF.

FRX-L is designed to produce compact, high-density, field-reversed plasma configurations with parameters compatible with what is needed to serve as a MTF target (deuterium) plasma that has a density of ~ 1×10^{17} cm^{-3} and a temperature of ~ 200 eV at magnetic fields of ~ 3 to 5 T and a lifetime of ~ 20 μs. The FRX-L uses four high-voltage capacitor banks (up to 100 kV, storing up to 1 MJ of energy, see Figure 2) to drive a 1.5-MA current in one-turn magnetic-field coils that surround a 10-cm-diam quartz tube (Figure 3) where the target plasma is formed. We use a suite of sophisticated plasma diagnostics to ensure that the target plasma has the correct density, temperature, lifetime, and purity needed for use in MTF. Multi-chord laser interferometry measures the plasma density; high-power laser scattering (Thomson scattering) is used to measure the plasma temperature and density; a variety of plasma spectroscopy measurements are taken to determine the plasma purity; sets of external magnetic probes measure the plasma shape and pressure; bolometers measure the power radiated from the plasma; and fast imaging cameras view the plasma symmetry and wall interactions.

The entire FRX-L experiment is controlled from a shielded screen room, and data from approximately 100 channels of measurements are acquired on high-speed digitizers before being transferred to a database for display after each shot. During a day of operations, 20 to 30 shots (each lasting about 100 μs) can be fired under computer control. A blast door/wall separates the researchers from the high-voltage and high-energy conditions in the experiment. Red and yellow warning lights indicate the status of the experiment; meanwhile, experienced researchers often plug their ears when they hear the building announcement "Main bank is charging"!

Presently, plasma parameters at a density of ~ 2 to 4 × 10^{16} cm^{-3}, temperatures of 100 to 250 eV, magnetic fields of 2.5 T, and lifetimes of 10 to 15 μs are within a factor of 2 to 3 of our desired endpoints for the starting target plasma. In the coming year, while also improving the pulsed power and plasma performance, we will begin translating these plasmas into a test-liner chamber to confirm the plasma cleanliness and lifetime and our ability to trap the plasma in the close-fitting aluminum liner.

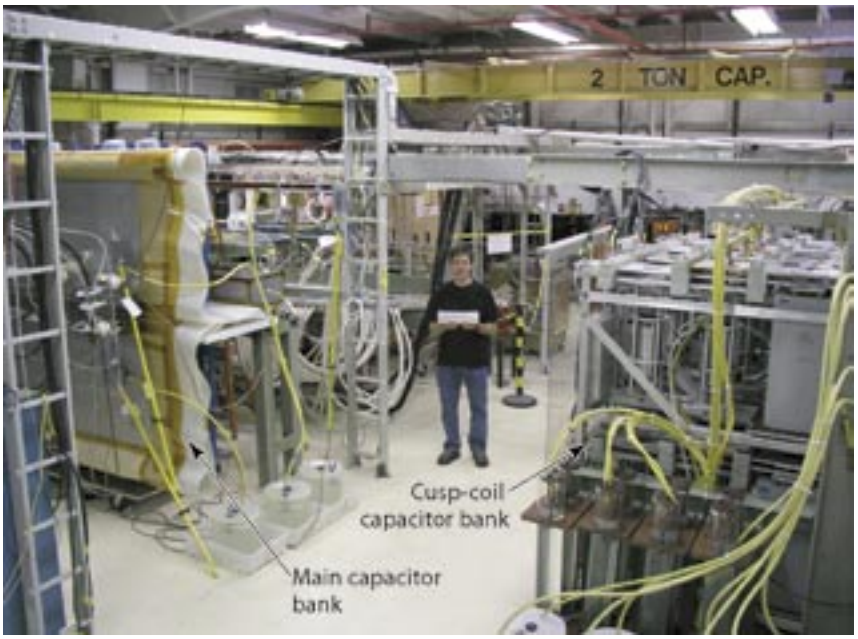

Figure 2. The FRX-L experimental bay, showing the pulsed-power electrical systems that supply energy to the plasma injector. Martin Taccetti (P-24) holds a full-scale aluminum liner in his hands. The main capacitor bank (to the left), delivers 1.5 MA of current to the theta pinch coils. Another bank (on the right) provides energy to the cusp coils.

Figure 3. The initial FRC target plasma is formed inside a small (10-cm-diam) quartz tube. One of our AFRL collaborators, Chris Grabowski, provides the scale for the target plasma by looking through the tube.

Conclusion

Recently we have submitted a proposed extension of the MTF project to DOE, which will authorize the goal of combining our plasma injector with the AFRL "Shiva Star" (Figure 4) liner-implosion system. With partners from the University of New Mexico, the University of Wisconsin, the University of Washington, and the AFRL, we plan to demonstrate fusion-relevant plasma conditions within this decade. The fusion plasma that we hope to produce (at a rate of about 1 shot per week in the laboratory) would be a clean deuterium plasma that will be confined by an enormous magnetic field of 500 T for about 1 μs and will reach a temperature of 5 to 8 keV and a density of ~ 1×10^{19} cm^{-3}! Success could lead to the first demonstration of break-even plasma conditions using magnetized targets in the Atlas liner-implosion facility at the NTS in later follow-on experiments.

References

1. See http://fusionenergy.lanl.gov/
2. R.E. Siemon, I.R. Lindemuth, and K.F. Schoenberg, "Why MTF is a low cost path to fusion," *Comments Plasma Physics Controlled Fusion* **18**(6), 363–386 (1999).
3. M. Tuszewski, "Field reversed configurations," *Nuclear Fusion* **28**(11), 2033–2092 (1988).
4. J.M. Taccetti, T.P. Intrator, G.A. Wurden, S.Y. Zhang *et al.,* "FRX-L: A field-reversed configuration plasma injector for magnetized target fusion," *Review of Scientific Instruments* **74**(10), 4314 (2003).

Acknowledgment

This work is supported by the DOE Office of Science, Fusion Energy Sciences Innovative Confinement Concepts Program, with experimental collaborators from the AFRL and with theory collaborators from LANL, General Atomics, and LLNL.

Figure 4. The AFRL pulsed-power machine "Shiva Star," which is about the size of two basketball courts, will be the site for the first combined LANL plasma injector and AFRL Shiva Star liner-implosion experiments earmarked for the 2006–2007 timeframe.

For more information, contact Glen Wurden at 505-667-5633, wurden@lanl.gov.

Neutron Generation Using Inertial Electrostatic Confinement

J. Park (P-24), R.A. Nebel (T-15)

We are developing a compact and portable neutron source based on the inertial-electrostatic-confinement (IEC) plasma device, located at TA-35, Building 27 at LANL. The system consists of highly transparent concentric grids (two or three grids) in a vacuum chamber (Figure 1). Plasmas containing deuterium and tritium ions are produced either by electron injection or by an inductively coupled antenna. Once a plasma is produced, a high-negative-voltage pulse is applied to the inner grid (- 100 kV for 1-ms duration) to accelerate the ions to the center of the vacuum chamber where they collide with each other and the background gases. The ion energy can achieve the full potential of the accelerating grid and thus reach very high energy (50–100 kV) where the fusion cross section becomes large and copious neutrons are produced.

Currently, the device is operated with two grids and uses only deuterium fuel. In the next phase of the project, we will use a mixture of deuterium and tritium to enhance the time-averaged neutron-production rate to > 1 x 10^{10} neutrons/s. The grid system has been recently upgraded with a tungsten-rhenium alloy that allows high-temperature operation; also a pulsed-discharge operation has been implemented to increase peak plasma performance. The goal of this project (in coordination with NIS-6) is to develop a compact, durable (> 5,000-hour lifetime) neutron source for an active nuclear assay of highly enriched uranium for homeland security and other applications. The project also includes a proof-of-principle test of a radical, yet promising, nuclear-fusion concept—the periodically oscillating plasma sphere (POPS)—for fusion-power production. We recently demonstrated the stability of the virtual cathode, which is a prerequisite for POPS, both experimentally and theoretically.

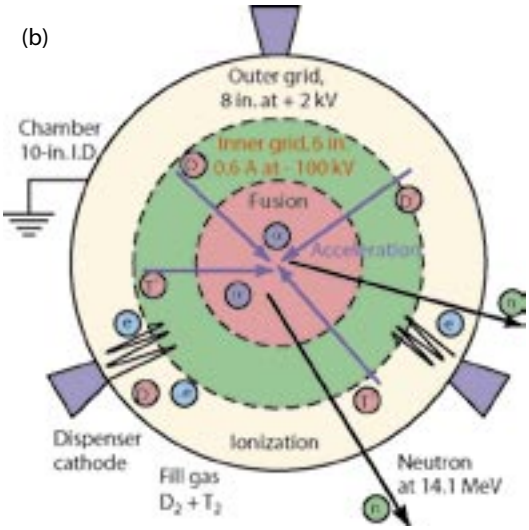

Figure 1. (a) Photos of the new grid system and (b) schematic of the IEC concept.

National Fusion Collaborations

G.A. Wurden, R.J. Maqueda, I. Furno (P-24)

We have off-site fusion collaborations at the University of Washington, Massachusetts Institute of Technology (MIT), and Princeton University. At the University of Washington, we focus on researching the physics of rotating magnetic-field current drive in an FRC plasma. In particular, we have been prototyping multichannel bolometers to measure the radiated power from the FRC plasma.

At MIT, we operate an infrared video-camera system, with a specialized zinc-selenide periscope system that allows us to get a view of the Alcator C-Mod tokamak divertor. Of particular interest is the flow of power onto different parts of the divertor during high-performance plasma operation.

At Princeton University's Princeton Plasma Physics Laboratory, we have been engaged in a study of turbulence in the edge of the National Spherical Torus Experiment spherical tokamak plasma. We operate two intensified, fast, video-camera systems, at rates up to 40,000 frames/s, and use them to view the edge of the plasma when a small gas puff is injected to "light up" the pre-existing plasma turbulence. This technique is called "gas-puff imaging" and allows us to see interesting differences in plasma transport of "blobs" between so-called "low-mode" and "high-mode" confinement regimes, which can then be compared to plasma models using computer simulations.

Combustion Enhancement of Propane by Silent Discharge Plasma

L.A. Rosocha, S.M. Stange (P-24), D. Platts (P-22), D.M. Coates (P-DO)

It is well known that the application of an external electric field to a flame can affect its propagation speed, stability, and combustion chemistry. External electrodes, arc discharges, and plasma jets have been employed to allow combustible-gas mixtures to operate outside their flammability limits by gas heating, injection of free radicals, and field-promoted flame stabilization. Other investigators have carried out experiments with silent electrical discharges applied to propagating flames. These have demonstrated that the flame-propagation velocity is actually decreased (combustion retarded) when a silent discharge is applied directly to the flame region, but that the flame-propagation velocity is increased (combustion promoted) when a silent discharge is applied to the unburned gas mixture upstream of a flame. Two other recent works have considered the possibility of combustion enhancement in aircraft gas-turbine engine combustor mixers by using a plasma-generating fuel nozzle that employs an electric-arc or microwave plasma generator to produce dissociated fuel or ionized fuel and pulsed corona-enhanced detonation of fuel-air mixtures in jet engines. In contrast to these prior works, we have employed a silent discharge plasma (SDP) reactor to break up large fuel molecules into smaller molecules and create free radicals or other active species in a gas stream before the fuel is mixed with an oxidizer and combusted.

Figure 2. A schematic of our SDP reactor "activating" the propane before combustion.

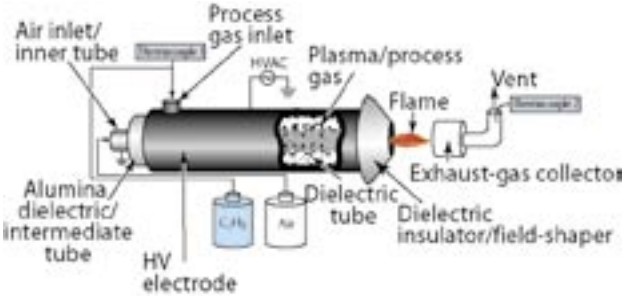

In our work, a cylindrical SDP reactor (Figure 2) was used to "activate" propane before mixing it with air and igniting the combustible gas mixture. With the plasma, the physical appearance of the flame changes, and substantial changes in mass-spectrometer fragmentation peaks are observed (e.g., propane fragments decrease and water and carbon dioxide increase). This indicates that the combustion process is enhanced with the application of the plasma. So far, we have acquired data on the plasma power, specific energy, and degree of combustion enhancement of propane as determined from our experiments with a coaxial SDP reactor. In the future, we would like to conduct experiments with more practical fuels (e.g., gasoline, diesel fuel, and jet fuel).

Neutron-Imaging Studies of Asymmetrically Driven Targets on the Omega Laser

C.R. Christensen (P-24), D.C. Wilson (X-2)

An experimental campaign, known as Asymmetric Direct Drive Spheres (ADDS), involved a series of studies designed to explore the relationship between asymmetry and the mix of capsule-shell material into the DT fuel during ICF implosions. To understand this relationship, we varied the energies of each of the 60 beams on the Omega laser at the University of Rochester to produce symmetric, prolate, or oblate implosions at DT fill pressures of 10, 5, or 2.5 atm.

During the experimental runs, we obtained simultaneous neutron (Figure 3) and x-ray images, and, together with neutron yield and ion temperature, compared them to predictions of ICF mix models. The agreement between our experiments and the ICF mix models is good for all three fill pressures. We expect that the data from the ADDS experimental campaign will be very useful in validating predictions of turbulent-mix models, which often involve quantities that are difficult to determine experimentally. By contrast, the yield proportion of the symmetric/prolate/oblate implosions leads to a testable criterion that depends only on simple geometric factors.

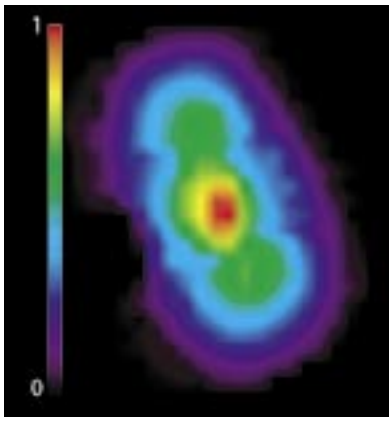

Figure 3. Reconstructed neutron image of a prolate implosion using 13% drive asymmetry.

Developing a Fundamental Understanding of Laser-Plasma Interactions

D.S. Montgomery, J.L. Kline, J.A. Cobble, J.C. Fernández (P-24), H.A. Rose, D.F. DuBois (T-13), B. Bezzerides, E.S. Dodd, D. Barnes, L. Yin, J. Kindel (X-1), H.X. Vu (University of California, San Diego)

Laser-plasma instabilities (LPIs) can severely limit the amount of laser power coupled into targets used to study high-energy-density (HED) physics and must be properly controlled in order to achieve fusion ignition for ICF experiments, such as those planned on NIF. Such instabilities occur when intense laser light scatters off of waves in the plasma, causing the amplitudes of the scattered light and plasma wave to grow exponentially at the expense of the incident laser power.

In realistic laser beams, such as those planned for NIF, the laser-beam intensity profile in the focal region consists of an ensemble of thousands of intense regions, called hot spots. Growth of instabilities occurs mainly in these intense hot spots, and an instability in one hot spot can seed instabilities in other hot spots. LPIs, in this case, can be highly complicated, where various instabilities can compete with one another and can also modify the local laser and plasma conditions, thus changing the conditions for instability growth. In NIF-scale targets, where the laser propagates through several millimeters of plasma, these detailed processes cannot be modeled from first principles because the laser-plasma system must be resolved at scales less than the wavelength of light. The system size is thousands of wavelengths long, and the required computing resources are beyond the reach of planned computers.

Our research focuses on understanding LPIs at the most fundamental level, within a single laser hot spot. This is realized in experiments using a nearly diffraction-limited laser beam at the Trident laser facility to drive instabilities in a preformed plasma. State-of-the-art physics models can simulate the volume of a single hot spot so that we can make direct comparison between numerical simulations and experiments. Additionally, the laser and plasma conditions in these experiments are extremely uniform—such that detailed structures associated with these processes can be resolved, allowing us to discriminate between various processes. One of the successes in 2003 was the observation of a transition from a wave-wave nonlinearity to a wave-particle nonlinearity for large-amplitude electron plasma waves (EPWs). These waves participate in stimulated Raman scattering (SRS), an instability important to laser fusion, and their nonlinear behavior largely determines how much laser power is lost to this unstable process. Using Thomson scattering, we detected the large-amplitude EPW driven by SRS. In a regime where the EPW wavelength was much larger than the Debye screening length, the SRS EPW drove a cascade of multiple EPWs via the Langmuir-decay-instability process, which was also detected by Thomson scattering. In a regime where the EPW wavelength was of the order of the Debye length, we detected a single frequency-broadened EPW. The amount of frequency broadening was consistent with a simple model for electrons trapped in the potential troughs of the EPW. Thus, the EPW nonlinearity transitions from a wave-wave nonlinearity to a wave-particle nonlinearity as the EPW wavelength approaches the Debye length. These observations are in qualitative agreement with numerical simulations and will allow us to better refine our models.

Experimental Investigation of Fundamental Processes Relevant to Fusion-Burning, Strongly Coupled, Multi-Material Plasmas

J.F. Benage, F.J. Wysocki, R.R. Newton (P-22), D. Montgomery (P-24), J.P. Roberts, G. Rodriguez, S.A. Clarke, A. Taylor (MST-10), M.S. Murillo, J.O. Daligault (T-15)

The goal of this project is to make a detailed experimental investigation of fundamental physical processes that occur in a fusion-burning, strongly coupled, multi-material plasma. When plasmas are rapidly heated to reach the conditions necessary for fusion to occur as in an ICF implosion capsule, the plasma conditions will relax to an equilibrium state. Because fusion reaction rates are very sensitive to temperature at low ion temperatures, a small error in the temperature can produce a much larger error in the fusion reaction rate. Thus, the relaxation toward equilibrium and the distribution of energy among plasma constituents could be significantly affected when and if the appropriate conditions for fusion are reached. In addition, because all laboratory fusion schemes require the containment of the plasma by some material other than the fusing particles, contaminant ions are always present in the plasma. These ions become highly ionized and can affect the plasma density and average charge Z. These contaminating ions also interact strongly with the other plasma species. When the interaction energy between the species becomes comparable to the thermal energy, the plasma is called strongly coupled. Unfortunately, such strongly coupled plasmas violate the assumptions made for theories used in modeling the plasma undergoing fusion. Thus, to improve our ability to predict and understand such fusion burning plasmas, we must have better models that are validated by experiment. Toward that end, we are conducting two experiments.

In our first experiment, an intense laser incident on a high-density gas jet creates hot plasma. Using Thomson scattering and absorption spectroscopy, we obtain time-resolved measurements of the electron and ion temperatures to determine the temperature equilibration rate between the electrons and ions in the strongly coupled plasma. In our second experiment, a very short-pulse laser produces a CH plasma and a gold plasma side by side. We obtain the rate of diffusion of light ions through heavy ions in the strongly coupled plasma by measuring the diffusion of the H ions through the gold plasma for various gold-plasma thicknesses. The results of these experiments will provide data to validate theoretical models that have been recently developed to describe these processes. When validated, such models can be incorporated into codes used to model, design, and predict the behavior of fusion-burning plasmas.

Applied-Science Internship Program

T. Intrator (P-24)

Fiscal year 2003 was the second year of existence for the Applied-Science Internship Program (ASIP) in P-24 and P-25 (http://education.lanl.gov/newEPO/CS/ASIP.html). ASIP is an undergraduate experimental training program that targets applied science and engineering skills—physics and engineering of lasers, pulsed power, accelerators, ICF, high-energy density physics, and weapons aspects of dynamic experimentation and diagnostics and underground experimentation. The goals of this program are to recruit students to LANL and rapidly train them to be contributors to the stockpile stewardship program, to develop and hire highly qualified students into LANL's critical-skills pipeline, and to provide a reliable source of exciting jobs and feedback on curriculum development for local institutions so that they can attract higher-quality students.

ASIP adds an essential component to our student pipeline by providing two avenues for recruitment to supply LANL's future workforce. First, continued support of students throughout their academic career increases

the likelihood that they will choose a career at LANL. Second, ASIP expands the process by networking with academia. The program focuses on near-term hires and on undergraduate- and graduate-level students. The large, continuing, year-round student population of ASIP has created a culture that is luring more high-quality students to LANL. ASIP is continually bombarded with excellent resumes elicited by word-of-mouth recommendations from alumni. Program leaders have found jobs for many students that they cannot hire themselves because of funding and space limitations. In P-24, 60% of the students return, stay for long-term internships, or do both. ASIP has reached the point at which expansion will be required to admit more new students. P Division is committed to hiring new staff members from the program. The Division will commit staff members to develop the curriculum; will provide staff support for curriculum development of associates, bachelors, masters, and doctoral degrees; and will recruit students to fill the program. ASIP is a joint venture among P Division, MST Division, and several institutions, including the New Mexico Institute of Mining and Technology, Socorro; MIT; and Northern New Mexico Community College (NNMCC).

In FY 2003, the ASIP program included 26 students and retained a record number of these students—11 out of 13 returned from the previous year's program in P-24 alone (Figure 4). The schools represented included MIT, Stanford University, Princeton University, NNMCC, Purdue University, the University of Michigan, Clarkson University, and the University of Pennsylvania. Eight students had fellowships from outside LANL. One student received a prize at the LANL student symposium for the best engineering poster presentation. Two are doing doctoral theses at LANL, and one is being groomed to become a technician next year. One student is the lead author on a paper that will soon appear in *Review of Scientific Instruments 2003* and another co-authored a paper that has already been published. Three are going to graduate school—two to the University of Wisconsin and one to the University of Nevada, Reno. Two are staying at LANL beyond the summer, and a large number of the FY 2003 students are expected to return in FY 2004. A 2003 Plasma Physics Summer School Seminar Series, which typically attracted more than 30 students per class, was coordinated with the Physical Sciences and the Dynamics Summer School (http://wsx.lanl.gov/RSX/summer-school/Summer_school_homepage.htm). The seminar series included talks on radiation hydrodynamics from an X Division staff member and talks about plasma physics, astrophysics, and experimental issues from P-24 staff members. ASIP organized a LANL-wide workshop on plasma astrophysics that drew more than 70 people. The program received an MIT UPOP (Under-graduate Practice Opportunity Program) Internship Excellence Award that carried with it a $2,000 stipend per MIT UPOP student who interned at P-24.

Figure 4. Students from the ASIP pose for a group photo at a summer 2003 "get together" at mentor Glen Wurden's home.

X-ray Diffusion Through a Thin Gold Wall

R.G. Watt, G. Idzorek (P-22), R. Chrien (X-2)

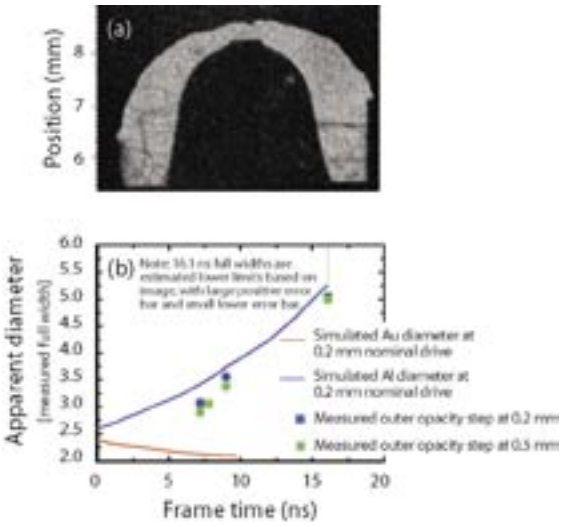

Figure 5. (a) A backlit radiograph of the expanding cylinder about 9 ns after peak radiation drive. (b) A time history of the radiographic measurements compared to threoretical predictions.

The transport of x-rays into or through the thin gold wall of a hohlraum is an energy-loss mechanism in indirectly driven ICF hohlraums. When using a thin-wall hohlraum (TWH) in ICF (which allows us to both reduce the material load on large optics and image the laser-wall interaction region through the wall), the loss mechanism may become significant. Assessing this loss requires obtaining correct simulation results, which in turn, requires having the correct physical models for radiation flow through the wall in the simulation code. Experimental data are needed to confirm that we used the correct models. In the absence of accurate experimental data, simulations might lead us to erroneous conclusions about the efficacy of TWHs for use in experiments at large laser facilities and ultimately on NIF.

Experimental data are being obtained using the Z accelerator at SNL to address this deficiency. A dynamic hohlraum is used to produce x-rays from a radiating volume with a 200-eV-equivalent radiation temperature to drive a TWH. The TWH is comprised of a thin gold layer (1 μm, somewhat thinner than the typical 2- to 3-μm gold layer in a normal TWH) supported on the outside by a 25-μm aluminum layer. The long duration of the drive and the limited thickness of the gold layer allow the radiation wave to break through the gold layer, after which the inward motion of the gold lowers the density below solid and allows diffusive radiation flow through of order 10 radiation mean-free paths in the gold before reaching the outer aluminum. Escaping radiation consequently heats the aluminum layer that surrounds the gold. The motion of the aluminum is used to study the diffusion of radiation through the gold in an integrated experiment in which the diffusion approximation should be valid in the gold. The primary diagnostic is an x-ray-backlit image of the expansion of the closed cylinder as a function of time. Comparison of the predicted and observed position of the outer surface of the aluminum wall provides a good measure of the model used in the calculations.

The expanding closed cylinder is driven by a 200-eV radiation source of 3- to 5-ns duration driven by a dynamic hohlraum with a 4-mm radiation exit hole (REH). The drive radiation from the pinch is transported upward 1.7 mm above the REH by a low-density, foam-filled gold cone to get it to the location of the physics package. Once inside the closed cylinder, the radiation escapes through the gold wall and heats the aluminum, which subsequently expands. The expanded aluminum is thick enough to significantly block 6.7-keV x-rays emitted from an iron back-lighter foil, which is illuminated by ~ 700 J of green laser light incident in about 0.6 ns over a 100-μm-diam focal spot. The image captured on x-ray film on the opposite side of the target from the back-lighter foil is captured inside a tungsten body camera on a series of films after being filtered through an iron filter pack to remove most of the radiation at energies less than 6 keV. The system resolution in this point-projection configuration is about 65 μm.

By comparing the outer aluminum wall's base diameter, the general shape of the aluminum-vacuum interface, and, ultimately, the transmission level of the back-lighter x-rays through the various regions of the hohlraum, we can assess how well the simulations match the measured data and thus attempt to verify the radiation-flow model and the opacity numbers used in the simulation. Figure 5(a) shows a backlit radiograph of the expanding cylinder at approximately 9 ns after peak radiation drive. The figure shows that the originally vertical sides below the hemispherical closed top have now expanded out conically. From a series of such images, we can compare the time history of the diameter at 200 μm above the bottom of the straight section, for instance,

with the predictions. This comparison is also shown in Figure 5(b). This work has shown both close general agreement with the generic behavior of the cylinder (suggesting the radiation diffusion process through the gold wall is being modeled adequately) and some differences that suggest somewhat different 6.7-keV x-ray transmission through the aluminum than anticipated. Continuing work on this experiment should further illuminate both the agreement and the discrepancies.

Radiation-Hydrodynamic Experiments on the Z Accelerator

P.A. Keiter, G.A. Kyrala (P-24), G. Idzorek, R.G. Watt (P-22), R.R. Peterson (X-1), P.J. Adams, R.E. Chrien, D.L. Peterson, B.P Wood, M.M. Wood-Schultz (X-2)

We performed radiation-hydrodynamic experiments using the Z accelerator at SNL. In these experiments, a radiation and shock front is launched in a cylindrical piece of low-density aerogel foam. The pre-shocked target was a 3-mm-long, 7-mm-diam cylinder of 23-mg/cc-density SiO_2 aerogel foam. Initially, these fronts co-propagate—but as the hohlraum temperature increases, the radiation front becomes supersonic and propagates faster than the shock front. The purpose of these experiments is to accurately characterize a relatively simple experimental configuration and to compare the results of the experiments with predictions from different codes. In the simulations, many parameters are varied, including foam density, radiation drive, opacity, and aperture size. Simulations with the RAGE code shows that the breakout of the radiation front is most sensitive to changes in the density of the foam and the radiation drive. X-ray radiography is used to determine the density of the targets and to determine how uniform the density of each target is. The uniformity of the target is important because if large non-uniformities are present, then the radiation front will propagate differently at different spatial locations.

The radiation drive is measured with both x-ray diodes and silicon diodes. These diodes are well calibrated so that the raw signal obtained by the diodes can be converted to a temperature. Silicon diodes also observe the front face of the foam target so that the break-out time of the radiation front can be measured. We have measured the shock shape and position with x-ray radiography. Figure 6 shows a typical radiograph from the experiment. A 6.7-keV iron backlighter is used to produce the diagnostic x-rays. These x-rays pass through the target and are absorbed according to the opacity of the material.

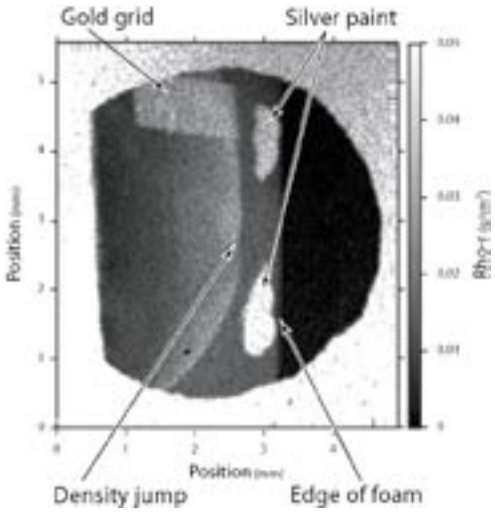

Figure 6. An x-ray radiograph of a 3-mm-long, 23-mg/cc-density foam target. The radiograph was taken 9.7 ns after the peak of the pinch radiation using a 6.7-keV iron backlighter. The opaque rectangle is a gold grid, whereas the two opaque ovals are from silver paint placed on the front surface of the foam; we believe the silver paint diffused into the foam.

Quick-Reaction Capability

C.M. Frankle (P-22)

The quick-reaction-capability project, operated by NIS Division's International Technology program office, provides funding for LANL personnel with particular expertise to assist the Joint Staff. When a specific request for assistance from a combatant commander is made to the Operations Directorate of the Joint Staff, the Joint Staff may request that a person with specific, applicable expertise from LANL be assigned to their office in the Pentagon for several months. The Joint Staff finds that having a technical expert onsite to help address a specific national-security issue is quite useful. Such problems are usually of immediate importance to the DoD and by their nature are generally highly classified. Christen Frankle (P-22) participated in such a rotation during the middle of 2003.